DEVELOPMENT OF LIGAND-OBSERVED METHODS FOR CHARACTERIZING PROTEIN-LIGAND BINDING WITH DNP-ENHANCED NMR

A Thesis

by

JIANDU HU

Submitted to the Graduate and Professional School of
Texas A&M University
in partial fulfillment of the requirements for the degree of

MASTER OF SCIENCE

Chair of Committee,	Christian Hilty
Committee Members,	Kevin Burgess
	Xin Yan
	Steven Wright
Head of Department,	Simon North

December 2021

Major Subject: Chemistry

ABSTRACT

Ligand-observed NMR has evolved into a powerful high-throughput screening (HTS) tool for drug discovery through characterization of protein-ligand interactions. Hyperpolarization created by D-DNP can improve the sensitivity of NMR by >1000x, enabling binding characterization at micromolar or sub-micromolar protein concentrations near physiological conditions. Incorporating D-DNP, ligand-observed NMR methods for characterizing binding are developed. The first method enables ^{1}H detection of strong binders through competitive binding. While direct observation of slowly exchanging ligands is challenging, we demonstrate that changes in R_2 of a reporter ligand can indirectly probe the binding of a strong competing ligand. The second method features ^{19}F-based detection of heteronuclear NOE created by polarization transfer from hyperpolarized water protons to ligand ^{19}F spins. Hyperpolarization of water broadens the applicability, allowing the study of ligands with poor polarizability. Characterization of real-time water signal enhancement, required for accurate quantification of cross-relaxation rates (σ), is accomplished with a purpose-designed dual-channel spectrometer.

ACKNOWLEDGMENTS

I would like to first thank my advisor and committee chair, Dr. Hilty, for providing me with the opportunity to work under his supervision. I am grateful for his willingness to offer hands-on learning and for his genuine interest in helping me become an autonomous researcher. I feel inspired by his diligence, passion, and dedication to research and impressed by his expertise in the field of NMR. Thanks to his guidance, I have gained not only skills related to the field but also inner strength, patience, and improved attention to detail. His determination in problem solving keeps motivating me to move forwards with tenacity at all times.

I also want to express my gratitude for my committee members, Dr. Burgess, Dr. Yan, and Dr. Wright for their support and guidance throughout the course of this research. They provided me with useful suggestions and care along the way. I also wish to acknowledge the departmental faculty and staff for making my time at Texas A&M University a great experience, especially Sandy Horton, whose unending support helped me through the most difficult times.

I must also thank all Hilty group members. Everyone was always willing to help me without hesitation and makes intellectual contributions to my projects. A special thanks goes to Chang Qi and Dr. Jihyun Kim for collaborations and encouragement. Days after days of running experiments, troubleshooting, and learning together nourished lasting friendships.

I also want to thank my undergraduate research advisor, Dr. Bradley Smucker, for his continuous encouragement and support throughout my study. He offered invaluable professional advice as I proceeded through the program.

Finally, I would like to recognize my friends and family, without whose support, I could not have gone this far. I am tremendously grateful that they were always here for me.

CONTRIBUTORS AND FUNDING SOURCES

Contributors

This work was supported by a dissertation committee consisting of Dr. Christian Hilty, Dr. Kevin Burgess, and Dr. Xin Yan of the Department of Chemistry, and Dr. Steven Wright of the Department of Electrical and Computer Engineering.

Chang Qi (C. Q.) and Dr. Yunyi Wang (Y. W.), fellow and former graduate students of the Department of Chemistry, contributed to the data collection and analysis in Chapter 2. C. Q. participated in collecting and analyzing the data for all experiments, and Y.W. assisted with collecting data for the control experiments. Dr. Baoyu Zhao (B. Z.), a postdoctoral scholar of the Department of Biochemistry and Biophysics under our collaborator Dr. Pingwei Li, expressed the protein and prepared the sample of the competing ligand used in Chapter 2. Dr. Jihyun Kim (J. K.), a former graduate student of the Department of Chemistry, contributed to the preliminary setup of the experiments described in Chapter 3, including instrumentation, sample preparation, and data analysis. Dr. Yue Zhu (Y. Z.), a former graduate student of the Department of Chemistry, helped troubleshoot the homemade spectrometer setup used in Chapter 3.

Funding Sources

Funding for this work was provided in part by an assistantship from Texas A&M University, the National Institutes of Health under Grant Number R01-GM132655, and the Welch Foundation under Grant Number A-1658.

NOMENCLATURE

1D	One Dimensional
2D	Two Dimensional
AMP	Adenosine MonoPhosphate
BBO	BroadBand Observe
cdG	cyclic di-GMP
CSA	Chemical Shift Anisotropy
CSP	Chemical Shift Perturbations
CPMG	Carr-Purcell-Meiboom-Gill
CW	Continuous Wave
Cryo-EM	Cryo-Electron Microscopy
D-DNP	Dissolution Dynamic Nuclear Polarization
DMSO	DiMethyl SulfOxide
DQ	Double-Quantum
EPR	Electron Paramagnetic Resonance
ESI-MS	Electrospray Ionization Mass Spectrometry
FP	Fluroescence (de) Polarization
GMP	Guanosine MonoPhosphate
HDX MS	Hydrogen/Deuterium eXchange Mass Spectrometry
HTS	High Throughput Screening

HSQC	Heteronuclear Single Quantum Coherence
INPHARMA	Interligand Noes for PHARmacophore MApping
ITC	Isothermal Titration Calorimetry
Laue XRD	Laue X-Ray Diffraction
MS	Mass Spectrometry
NMR	Nuclear Magnetic Resonance
NOE	Nuclear Overhauser Effect
NOESY	Nuclear Overhauser Effect SpectroscopY
PRE	Paramagnetic Resonance Effect
RD	Relaxation Dispersion
RF	Radio Frequency
RX	Receiver
SAXS	Small-Angle X-ray Scattering
SPR	Surface Plasmon Resonance
SQ	Single-Quantum
STD	Saturation Transfer Difference
STING	STimulator of InterfereN Genes
STING CTD	STimulator of InterfereN Genes C-Terminal Domain
TEMPOL	4-hydroxy-(2,2,6,6-TetraMethylPiperidin-1-yl) Oxy
TFBC	4-(TriFluoromethyl) Benzene-1-Carboximidamide
TINS	Target Immobilized NMR Screening
tr-NOE	transferred Nuclear Overhauser Effect

TROSY	Transverse Relaxation-Optimized SpectroscopY
TXI	Triple resonance Inversion
Water-LOGSY	Water-Ligand Observed via Gradient SpectroscopY
ZQ	Zero-Quantum

TABLE OF CONTENTS

Page

LIST OF FIGURES

Page

LIST OF TABLES

Page

CHAPTER 1

INTRODUCTION

1.1. Fundamentals

1.1.1. Significance of Protein-ligand Interactions

Protein-ligand interactions are pivotal to the realization of biological functions vital to the basic operation of living organisms. Molecular recognition between the macromolecules and ligands of high specificity and affinity provides the basis for the formation of protein-ligand complexes. These complexes perform various functions in cells: signal transduction upon ligand binding to transmembrane receptors, catalysis of enzymatic reactions, stimulation of an immune response based on antigen-antibody binding, etc.[1] Studying protein-ligand interactions is also central to drug discovery that requires the screening and evaluation of interactions between various pharmaceutical leads and protein drug targets in search of high-affinity ligands. The significance of protein-ligand interactions therefore demands a detailed understanding of their underlying mechanisms on a molecular level, as well as the development of characterization tools that facilitate such understanding.

1.1.2. Mechanisms of Protein-ligand Interactions

The mechanism of protein-ligand interactions is often investigated from the perspective of binding kinetics, thermodynamics, and binding driving forces. In terms of binding kinetics, the association and dissociation of a ligand molecule *L* from a protein binding partner *P* is a dynamic equilibrium that can be described as the following for proteins with a single binding site.

$$P + L \underset{k_{off}}{\overset{k_{on}}{\rightleftharpoons}} PL$$

where PL is the protein-ligand complex, k_{on} and k_{off} are association and dissociation rate constants of the forward binding and reverse dissociation reaction. The dissociation constant K_D at equilibrium can be expressed as a ratio in terms of rate constants or equilibrium concentrations, symbolized by square brackets, of corresponding molecular species. It is the reciprocal of the association constant K_A and can be defined as follows:

$$K_D = \frac{1}{K_A} = \frac{k_{off}}{k_{on}} = \frac{[P][L]}{[PL]} \tag{1.1}$$

When both K_D and the total concentrations of ligand $[L]_t$ and protein $[P]_t$ are known, the concentration of the PL complex at equilibrium, [PL], can be determined.[2]

$$[\mathrm{PL}] = \frac{[L]_t + [P]_t + K_D - \sqrt{([L]_t + [P]_t + K_D)^2 - 4[L]_t[P]_t}}{2} \tag{1.2}$$

The fraction of bound ligands (χ_b) can be calculated as $[PL]/[L]_t$, and the remainder is the fraction of free ligands ($\chi_f = 1 - \chi_b$). For most protein-ligand interactions, the association reaction is diffusion-controlled. In other words, k_{on} is typically governed by the rate of diffusion and takes on a value between 10^7 and 10^9 M^{-1} s^{-1}. Therefore, K_D is often approximated using knowledge of k_{off}.

The law of thermodynamics dictates the behavior of energy changes and heat exchange in a complex system composed of protein, ligand, and solvent. The driving forces behind association are a combined effect of various interactions and energy exchanges in the system. Gibbs' free energy (ΔG) is a key factor that affects driving forces, as a decrease in ΔG drives the protein folding and formation of the PL complex. In addition, the stability of this complex is conditioned by ΔG and increases with the magnitude of negative ΔG. Binding enthalpy (ΔH) and entropy (ΔS) are the two thermodynamic quantities that dictate the magnitude and sign of ΔG. Binding enthalpy

is largely affected by the formation of noncovalent interactions in the binding pocket that induces a large negative change in enthalpy. Binding entropy in a thermodynamic system consisting of protein, ligand, and solvent can be termed based on three sources of contribution.[3]

$$\Delta S = \Delta S_{solv} + \Delta S_{conf} + \Delta S_{r/t} \quad (1.3)$$

ΔS_{solv} is a positive entropy contribution from releasing solvent molecules upon binding, ΔS_{conf} accounts for the entropy change due to confirmation change, and $\Delta S_{r/t}$ is a negative contribution from the loss of rotational and translational freedoms upon binding. To create a highly stable PL complex, more negative change in ΔH and positive change in ΔS is desirable. Unfortunately, a gain in either entropy or enthalpy is often accompanied by a penalty in the other.[3] Association reduces ΔH but results in restricted mobility that makes ΔS smaller. Conversely, dissociation increases ΔS by releasing more molecules but causes an increase in ΔH due to the energy cost of disrupting noncovalent interactions. In rational drug design, optimization strategies often center around maximizing enthalpy/entropy gains while minimizing penalties. With the importance of these parameters in mind, the development of technological tools for characterizing protein-ligand interactions becomes a critical task.

1.2. Characterization of Protein-ligand Interactions

1.2.1. Tools for Characterizing Protein-ligand Interactions

There is an array of characterization techniques that provide different aspects of information about protein-ligand interactions, allowing the assessments of binding affinity, kinetics, thermodynamics, driving forces, and structural parameters.

Structures of protein-ligand complexes and unbound proteins can be elucidated at an atomic or near-atomic resolution with techniques including X-ray crystallography, Laue X-ray

diffraction (Laue XRD), cryo-electron microscopy (Cryo-EM), small-angle X-ray scattering (SAXS), and nuclear magnetic resonance (NMR). A few of them also provide access to the binding dynamics between the free and bound states: Laue XRD, for example, reveals the timescale of local motions and kinetics in addition to the structural determination.[4] SAXS informs about the equilibrium state, association/dissociation processes, and stoichiometry of binding. NMR allows the investigation of protein-ligand dynamics at a wide range of timescale from picoseconds to seconds.[5] There are disadvantages to each of these techniques. The requirement of sample crystallization for X-ray crystallography and Laue XRD challenges the characterization of proteins that resist crystallization. Cryo-EM and SAXS, despite their ability to directly determine structural ensemble, provide no information about the timescale of confirmation changes.[6] With solution-state NMR, structural elucidation for larger proteins can be challenging.

Computational methods such as docking and binding free energy calculations are introduced to complement empirical data. Protein-ligand docking, a common strategy used for structure-based drug design, applies search algorithms to screen through libraries.[7–9] It utilizes scoring functions to produce rapid predictions on the binding poses and affinity of a ligand to the protein target for selecting potential ligand candidates. Applying the principles of statistical thermodynamics, binding free energy calculation conducts thermodynamic averaging over a large pool of sampled confirmations to provide a computational result of free energies for a system of interest.[3,10] In contrast to the docking method, this approach focuses more on determining the energetic and entropic contributions instead of binding strength and orientation. In general, computational methods are economical, but the trade-off is the requirement of a large amount of computational time.[3]

Determination of binding affinity and specificity typically relies on one of the following tools: isothermal titration calorimetry (ITC), surface plasmon resonance (SPR), mass spectrometry (MS), Fluorescence (de) polarization (FP), and NMR.[3,11] ITC measures the heat transfer upon titration of a protein solution at various ligand concentrations in an isolated chamber,[12] enabling determination of binding constant, stoichiometry(n), and thermodynamic parameters (including ΔG, ΔH, ΔS, and heat capacity ΔC_p) of binding in the native state of protein without the need of immobilization or labeling. With a direct measurement of heat exchange at a constant temperature, ITC maps a quantitative, comprehensive thermodynamic profile for protein-ligand interactions, making it one of the most reliable and sensitive methods for evaluating the stability of protein-ligand complexes and binding driving forces. ITC, however, is inadequate when the binding exhibits slow kinetics or small change in enthalpy, or when macromolecules are difficult to be prepared at a large quantity.[13]

SPR measures small changes in the refractive index near the surface of an affinity biosensor so that the interaction between an immobilized component and analyte solution can be characterized.[3,14,15] It provides real-time kinetic measurements on the rate constants (k_{on} and k_{off}) and affinities in the range of $K_D = 10^{-3} – 10^3$ nM, from which thermodynamic quantities can be estimated. Compared to ITC, SPR is capable of characterizing ligands of higher affinity with a smaller quantity of protein, but there is the concern about altering the nature of protein-ligand interactions with immobilization.

MS informs about the stoichiometry and dissociation constant (K_D) of binding by analyzing the mass-to-charge (m/z) ratio of an ionized counterpart.[3,16] With MS, high sensitivity can be achieved with a small quantity of protein. Recent advancement in native MS, which produces

gentle desolvation of protein-ligand complexes under non-denaturing conditions, has enabled precise determination of molecular weight for complexes dominated by noncovalent interactions.[17] Hydrogen/deuterium exchange MS (HDX-MS), an emerging technique that monitors the exchange rate between protons and the deuterium on protein amide groups, has shown capability of identifying binding sites and structural changes upon binding.[18] Comparison MS studies between the gas and solution phase of the complexes can provide additional insights into the binding driving forces and the role of solvation in protein-ligand interactions.[19]

FP exploits different rotational properties of plane-polarized fluorescent light between the free and bound states of a ligand to determine binding affinity or thermodynamics.[3] In FP experiments, small molecules that tumble faster than the lifetime of the excited state of the fluorophores (typically nanoseconds) experience faster depolarization and result in more detected light to be unaligned with the plane of excitation.[20,21] Different from SPR and ITC, FP only involves inexpensive instrumentation, fewer reagents, and a smaller quantity of protein. Its nondestructive nature allows the equilibrium to remain undisturbed and repetitive measurements to be made with the reused plate. Nevertheless, the affinity measurements by FP are more likely to be affected by experimental conditions when interference from autofluorescence and light scattering is strong, or when labeling ligand with fluorophores alters the nature of an interaction.[21]

1.3. NMR as a Tool of Characterization

1.3.1. NMR Observables

NMR is a versatile and powerful tool for characterizing protein-ligand interactions, as it provides information about the affinity, dynamics, and structural constraints of an interaction. While many other techniques are restricted to characterization of high-affinity interactions, NMR

has demonstrated exceptional ability in investigating systems of various affinities.[11] In solution-state NMR, protein-ligand interactions can be studied under near physiological conditions. Another advantage of NMR is that site-specific information about the binding pocket can be obtained.[22]

Characterization of protein-ligand interactions with NMR is possible by observing signals from biomacromolecules or chemical compounds, which are, respectively, used for protein-observed or ligand-observed NMR.[2] NMR probes protein-ligand interactions by observing the difference in magnetic properties between the free and bound state. This results in perturbations of NMR-sensitive parameters upon binding that can be manifested as a change in chemical shifts, relaxation rates, NOE, linewidth, diffusion, exchange of saturation, and others. Chemical exchange, a dynamic process of ligands associating and dissociating from the protein, can directly affect some of these observables. The exchange rate (k_{ex}), which measures the average number of stochastic exchange events per unit time, can be expressed as $[P]k_{on} + k_{off}$. By comparing it against the difference in nuclear precession frequencies between the free and bound state of a molecule ($\Delta\nu = | \nu_f - \nu_b |$), the exchange regime can be assigned.[11] The regime is in a fast exchange regime if $k_{ex} >> | \Delta\nu |$, a slow exchange regime if $k_{ex} << | \Delta\nu |$, and an intermediate exchange regime in-between. The difference in chemical shifts between the free and bound state depending on the exchange rate can be used as an indicator of binding for both protein-observed and ligand observed NMR methods. Molecules in fast exchange are weakly bound (K_D > 10 μM and k_{off} >10^3 s^{-1}) and produce a population-weighted chemical shift with a narrow linewidth at a frequency of $\chi_f \nu_f + \chi_b \nu_b$, where χ_f and χ_b are the fraction of free and bound molecules, respectively. Molecules in slow exchange are tightly bound (K_D < 1–10 nM and k_{off} ~ 0.1–1 s^{-1}) and produce two distinct peaks near ν_f and ν_b. Changes in the observed transverse relaxation rate constant (R_2) of the ligand

upon binding are more prominent than changes in the R_2 of the protein and are often exploited to probe protein-ligand interactions in ligand-observed NMR methods. For ligands exchanging at a faster timescale than the spin relaxation, the R_2 of the ligand signal at the population-weighted chemical shift can be described with a two-state model of L↔P dynamics using the following equation.[23]

$$R_{2,obs} = \chi_f^L \nu_f + \chi_b^L \nu_b + \left(\chi_f^L X_b^L\right)^2 (2\pi\Delta\nu)^2 / k_{off} \quad (1.4)$$

In the slow exchange regime, the observed R_2 signals for the free and bound ligands based on a two-state model can be determined as follows:[24]

$$R_{2,f}^{obs} = R_{2,f} + [P]k_{on} = R_{2,f} + \chi_b^L k_{ex} \text{ (free ligand)}$$

$$R_{2,b}^{obs} = R_{2,b} + k_{off} = R_{2,b} + \chi_f^L k_{ex} \text{ (bound ligand)} \quad (1.5)$$

$R_{2,f}$ and $R_{2,b}$ are transverse relaxation rate constants of free and bound ligands in the absence of exchange, respectively. The linewidth, which is defined as the signal width at half height, can further be derived from the observed R_2 values for both free and bound ligand when the exchange is slow.

$$\Delta\nu = \left|R_{2,f}^{obs} - R_{2,b}^{obs}\right| / 2 \quad (1.6)$$

Under the typical experimental condition of [P] << [L], ligands in slow exchange bind to the protein strongly, causing binding sites to be saturated with a small fraction of bound ligands while the majority remains unbound. This disparity in the population and linewidth difference of free and bound ligands is so large that the bound signal becomes undetectable under slow exchange. A complete description about the effect of chemical exchange on magnetization is provided by the McConnell equation,[25] from which the chemical shift and relaxation rates can be numerically determined.

1.3.2. NMR Screening Methods

Protein-observed NMR

Most protein-observed NMR methods utilizes the observation of chemical shift perturbations induced by chemical exchange and intermolecular interactions. Most experiments based on observation of proteins utilize 2D heteronuclear correlation spectroscopy such as heteronuclear single quantum coherence (HSQC).[11,26] The individual proton signals of the protein can be resolved from their correlation to a different nucleus. However, the common nuclei that exist in proteins, ^{15}N and ^{13}C, merely have a natural abundance of 0.37% and 1.1%, respectively. Isotopic enrichment strategies such as uniform labeling or amino acid specific labeling thus are often required for protein-observed experiments. One highlighted merit of protein-observed methods is its ability to provide structural characterization of binding sites, which is essential for the optimization of pharmaceutical leads. If signal assignments are known, information about the interacting sites and the orientation can be determined for elucidating the structure of a binding epitope. With the use of amino acid specific labeling, limited structural information can be accessed even in the absence of signal assignments. Another benefit of using protein-observed approaches is that its applicability is not limited to ligands in fast exchange. Strongly binding ligands with K_D in the nanomolar range are difficult to directly characterize with ligand-observed methods but can be detected by observing the macromolecules.[27] A disadvantage is that a protein concentration of 20 – 200 μM, an order of magnitude higher than that for the ligand-observed methods, is typically required.[11,28] The size of the protein is limited to < 30 kDa for most protein-observed experiments that use uniform labeling due to severe line broadening in larger proteins. This limit can be expanded to near 100 kDa with amino acid specific labeling, where selective types of residues concentrated in the binding sites are labeled to reduce the spectral complexity.

The development of transverse relaxation-optimized spectroscopy (TROSY), where the destructive interference between dipolar coupling and chemical shift anisotropy causes partial suppression of T_2 relaxation in specific molecular geometries, has enabled the high-resolution study of large proteins with molecular weight of >100 kDa.[29]

Ligand-observed NMR

Owing to its simplicity, broad applicability, and relatively high sensitivity, ligand-observed NMR appeals as a high-throughput screening (HTS) approach. Ligand-observed NMR experiments eliminate the need for isotopic labeling and are applicable to detect binding to proteins of various sizes.[30] Such experiments also allow the observation of interactions at a considerably lower protein concentration (5 – 50 μM) than in most protein-observed studies. The scope of applicability for most ligand-observed methods is restricted to ligands in the fast or intermediate exchange regime. Detection of high-affinity ligands with K_D < 1 μM is likely to produce false negative signals, as signals of bound ligands are overwhelmed when the majority of ligands are free. Competitive binding is commonly employed as a complementary strategy for detecting strong binders, where a reporter ligand of weak or intermediate affinity is used to "spy" on the ligand of interest.[31] The foundation of most ligand-observed methods is the observation of either changes in NMR parameters or intermolecular magnetization transfer from the protein to ligand.

1.3.3. Introduction to Ligand-observed NMR

Ligand-observed approaches generally utilize the perturbations on the chemical shifts, relaxation, or NOE of the ligand signals to identify binding interactions. Methods based on binding-induced chemical shift perturbations (CSP) of a ligand upon binding are widely applied for screening applications due to the requirement of short acquisition times. Information about the K_D can be accessed from NMR-based chemical shift titrations. Screening through ^{19}F chemical shift perturbations for identifying potential drug candidates in a compound library has been demonstrated as effective with the advantage of less signal overlap due to the large chemical shift dispersion of ^{19}F signals.[32] While the chemical shift perturbations can be applied for screening with ^{1}H NMR, small changes in the chemical shifts relative to the signal broadening might be difficult to observe.[11] Experiments based on the relaxation effect therefore have been more extensively used. Relaxation is the process of nuclear spin polarization returning to Boltzmann equilibrium toward the direction of the magnetic field after perturbations of NMR pulses.[33] There are different mechanisms through which relaxation can occur, including dipolar interactions, chemical shift anisotropy (CSA), J-coupling, quadrupolar interactions, and others. The dipolar interaction between magnetic moments of two nuclei is responsible for the processes of auto relaxation and cross relaxation described by the Solomon equations.[34] The classic longitudinal or spin-lattice (T_1), involving the restoration of magnetization in the *z*-direction through auto relaxation, is known for determining the interval between NMR acquisitions. Cross relaxation is a process of magnetization transfer from one spin to another, giving rise to the nuclear Overhauser effect (NOE). Transverse or spin-spin (T_2) relaxation is the decay of magnetization in the *x*-*y* detection plane due to phase decoherence of nuclear spins over time. Methods that detect binding through the perturbations in T_1 or T_2 relaxation are termed as “relaxation-based” here, while those

that make use of the change in NOE are categorized as "NOE-based". All of these ligand-observed methods exploit different rates of rotational tumbling motion depending on the molecular size.

The rotational correlation time (τ_c) describes the time needed for the root-mean-square (rms) deflection of molecules to be one radian. It is characteristic of Brownian rotation diffusion of a particle in solution. According to the Stokes-Einstein-Debye relation, τ_c increases with molecular size.[35] Most ligands have a molecular weight of less than 1000 Da, exhibiting fast tumbling and short correlation time. In contrast, most proteins have molecular weight of over 10 kDa, exhibiting slow tumbling and long correlation time.[11] Ligands in a bound complex take on the tumbling behavior of macromolecules and show a drastic increase in τ_c compared to free ligands. The spectral density function $J(\omega, \tau_c)$, which describes the probability of finding motions at a given angular frequency ω, can be used to express relaxation rates. The normalized spectral density with a single correlation time that eliminates the effect of fluctuating local field can be written as follows:[36]

$$J(\omega, \tau_c) = \frac{2\tau_c}{1 + (\omega\tau_c)^2} \tag{1.7}$$

Transitions between different energy levels of a spin system occurs when the frequency of nuclear spin precession ω matches the Larmor frequency ω_0, the rate of natural spin precession in an external magnetic field. Since the maximum J value at a given τ_c occurs when ω approaches zero, relaxation parameters that depend on $J(0)$ can provide the best contrast upon binding. With their dependence on $J(0)$, dipolar [^{1}H, ^{1}H] R_2 relaxation ($R_{2,DD}$) and cross relaxation rates (R_{cross}) are two excellent parameters for probing binding.[33]

$$R_{2,DD} = \frac{1}{20} b^2 \big(5J(0) + 9J(\omega_0) + 6J(2\omega_0)\big)$$

$$R_{cross} = \frac{1}{10} b^2 \big(J(0) - 6J(2\omega_0) \big)$$

$$\text{with} \quad b = \frac{\mu_0 \hbar \gamma_H^2}{4\pi r^3} \tag{1.8}$$

μ_0 is the vacuum permeability, $\hbar$ is plank constant, γ_H is the gyromagnetic ratio of ^{1}H spins, and r is the distance between two nuclei. The principle of "relaxed-based" methods is the observation of a faster R_2 relaxation for bound ligands due to an increase in molecular weight and correlation time. "NOE-based" methods utilize the difference in cross-relaxation properties of ligands to identify binding interactions. With a short correlation time ($\tau_c\omega << 1$), free ligands in fast tumbling show a negative R_{cross} that translates to weak positive to no NOE depending on the molecular size. With a long correlation time ($\tau_c\omega >> 1$), proteins exhibit a positive R_{cross} and large negative NOE. Ligands form a complex of high molecular weight upon binding and consequentially exhibit the NOE properties of macromolecules that is indicative of binding.

1.3.4. "Relaxation-based" Methods

"Relaxation-based" methods identify binding by characterizing the difference in the intrinsic R_2 and signal linewidth between free and bound ligands. The Carr-Purcell-Meiboom-Gill (CPMG) pulse sequence is the most fundamental tool for intrinsic R_2 determination, consisting of a 90° pulse followed by spin echoes $[\tau - 180° - \tau]_n$, where τ is the delay between the 90° excitation pulse and a successive 180° refocusing pulse.[37] At each interval of 2τ, a refocused "spin echo" is created to eliminate the external effect of field inhomogeneity and random translational diffusion on R_2. The intensity of spin echoes decays over time as a result of intrinsic transverse relaxation. An exponential fit can be applied to the intensities of these echoes, from which the R_2 is determined. Conventional CPMG experiments are often coupled with titration experiments at different ligand and protein concentrations to provide an estimation for the thermodynamic

parameter K_D. There is a type of "relaxation-based" methods that exploits the paramagnetic resonance effect (PRE), which significantly increases the R_2 rate due to dipolar interactions between the nucleus and the unpaired electrons from a paramagnetic center. PRE methods have been applied to search for ligands binding to a secondary binding site and used to obtain long-range distance (>6Å) information.[38] Target immobilized NMR screening (TINS) has been introduced as a method to enhance the contrast of R_2 by immobilizing the protein target on a surface such as beads.[39,40] The amount of protein required by TINS is significantly reduced, as ligands can be passed through a reused protein sample multiple time. In general, methods that focus on the observation of R_2 are simple and efficient, making them an indispensable tool for HTS.

1.3.5. "NOE-based" Methods

Another class of ligand-observed NMR methods is "NOE-based", which relies on observation of changes in NOE or cross-relaxation rates upon binding. The NOE for free ligands in fast tumbling yields negative cross peaks (off-diagonal) in a 2D nuclear Overhauser effect spectroscopy (NOESY) spectrum, while ligands bound to macromolecules show positive cross peaks.[11] This is a result of different NOE buildup rates between free (200 – 1000 ms) and bound (50 – 100ms) ligands during the mixing time, a time delay before two pulses during which NOE builds up. Because the magnitude of NOE has an r^{-6} dependence to the distance between two neighboring spins, additional information about the binding structure can be extracted from NOE signals of neighboring spins.[40] However, the effect of NOE only produces a small change of a few percent in the signal intensity of a target spin, thus requiring longer experimental time or sensitivity enhancement.[41,42]

There exists an extensive number of "NOE-based" methods. Some representative examples include transferred NOE (tr-NOE), interligand NOEs for pharmacophore mapping (INPHARMA), saturation transfer difference (STD), and water-ligand observed via gradient spectroscopy (water-LOGSY).[11] Tr-NOE experiments measure the intra-ligand NOE from pairs of ligand spins that builds up during a mixing time, which is of opposite sign for free versus bound ligands.[43] The change in cross-relaxation rates of the two ligand spins upon binding can be quantified using the Tr-NOE method. By varying the mixing time, changes in the NOE signal can reveal additional information about the bound conformation and interaction sites of a ligand, as the interacting distances between different ligand spins and the protein yields NOE signals of different intensities depending on the mixing time. Its ability to provide structural characterization makes Tr-NOE an important tool for the optimization of pharmaceutical leads.[44]

INPHARMA is a method capable of characterizing the inter-ligand NOE effect between two ligands that competitively bind to the same binding pocket.[45,46] Magnetization transfer from spins of one ligand to those of the competing ligand is mediated by the protein spins. Knowledge about the orientation of the first ligand allows the indirect mapping of the binding pocket of a macromolecule, which is crucial for structure-based drug design.

STD, one of the most sensitive methods for binding characterization, is based on the spectroscopic difference between an on- and off-resonance spectrum as a result of magnetization transfer from the pre-saturated protein to bound ligands.[47,48] In STD experiments, an on-resonance spectrum is acquired by applying a frequency-selective pulse on the protein-only resonance to saturate protein protons, meaning that the population difference between ground and excited states of protein spins to approaches zero and the signal from these spins is suppressed. The saturation first spreads to the protons in proximity and then to the entire protein molecule due to the efficient

spin diffusion and fast cross relaxation of macromolecules, resulting in a nearly complete loss of protein signals. Partial saturation is received by ligands in the bound complex, and its magnitude differs for each ligand spin depending on its proximity to the protein. This difference can be interpreted for determination of ligand binding epitope by observing the change in buildup at varying saturation times. To measure an off-resonance spectrum, the pulse is applied to a region far off from the protein resonance so that no saturation is applied to the protein. The on-resonance spectrum is then subtracted from the off-resonance reference to yield an STD spectrum, where only signals from bound ligands are observed. STD is a preferred method for studying larger protein targets of >30 kDa, as the saturation transfer is more effective when the size of the protein increases. In addition, the use of ligands in large excess to the protein target allows the required protein concentration to be reduced.

Instead of directly saturating the protein, Water-LOGSY experiments apply saturation to bulk water protons.[11,49] Magnetization from water to ligand spins can be directly transferred from water molecules in the binding pocket or mediated by the protein that receives its magnetization via chemical exchange or intermolecular NOE with water protons before the magnetization is rapidly distributed through efficient spin diffusion. When interacting with inverted water magnetization via dipolar interactions, free ligands possess positive cross-relaxation rates that appear as negative NMR signals, whereas bound ligands exhibit negative cross-relaxation rates that correspond to positive NMR signals in a water-LOGSY spectrum. Water-LOGSY is well suited for studying low proton density receptors such as nucleic acids and highly solvated proteins.[49] In addition, the accessibility of ligands to solvent can be evaluated with water-LOGSY and be used to prevent false positive signals due to aggregation. Collectively, these “NOE-based”

methods have benefited drug discovery by enabling detection of binding, estimation of binding affinities, and structural determination.

1.4. NMR Sensitivity

In recent decades, NMR spectroscopy has evolved into a preeminent technique for studying protein-ligand dynamics and elucidating biomolecular structures at an atomic resolution.[50] The problem of low sensitivity, however, has limited its ability in answering biological questions with proteins or components that are difficult to purify or prone to aggregate at high concentrations. The intensity of NMR signals is dictated by nuclear spin polarization. For a nucleus with spin quantum number $I = 1/2$, two Zeeman energy levels are formed in a static magnetic field B_0 as shown in Figure 1.1. The difference in energy between these two states (ΔE) can be determined as below, where $\hbar$ is Plank's constant and γ is the gyromagnetic ratio.[33]

$$\Delta E = \hbar \gamma B_0 \tag{1.10}$$

Nuclear spin polarization (p), the population difference between spin states in a magnetic field, is dictated by Boltzmann's distribution. For a two-spin system, it can be calculated using the following equation.[33]

$$p = \frac{n_\alpha - n_\beta}{n_\alpha + n_\beta} = \frac{1 - e^{-\Delta E/k_B T}}{1 + e^{-\Delta E/k_B T}} = tanh\left(\frac{\gamma \hbar B_0}{2 k_B T}\right) \tag{1.11}$$

Here, n_α and n_β are the number of spins in the α and β states, respectively. k_B is Boltzmann's constant and T is temperature in Kelvin. The field strength and gyromagnetic ratio both contribute positively to the polarization level, whereas a higher temperature yields a lower polarization. The polarization level of most common nuclei such as ^{1}H and ^{13}C is typically around 10^{-5} near room temperature under a magnetic field of 9.4 T.

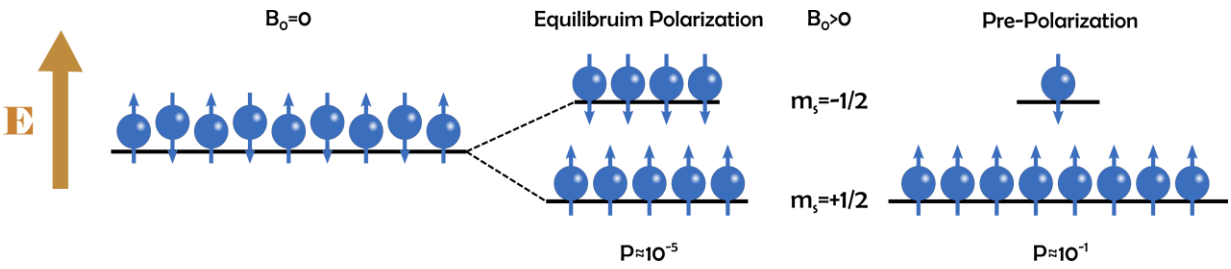

Figure 1.1 Effect of Zeeman splitting for a nucleus with ½ spin and the resulting nuclear spin polarization under Boltzmann equilibrium versus after hyperpolarization.

Efforts have been made to improve the NMR sensitivity from different aspects. The magnetic field strength has been improved by ~ 50 times since the invention of the first commercial NMR. Under a 32 T magnetic field provided by the strongest superconducting magnet available, the increase in sensitivity is about 3-fold.[51] The introduction of cryoprobes, which allow sample coils and electronics to operate at the cryogenic temperature while the sample is maintained in the ambient environment, can also provide a 3 – 4 fold increase.[52] In addition to the hardware modification, pulse sequences that allow the polarization transfer from high γ spins to low γ spins can enhance the NMR signals by a few fold.[53] However, a significantly large increase in sensitivity can be obtained with hyperpolarization techniques such as D-DN. Hyperpolarization is a process of creating nonequilibrium polarization by enlarging the population difference between spin states, leading to an increase in the NMR sensitivity by several orders of magnitude.[54] The incorporation of hyperpolarization techniques has allowed conventional NMR to overcome its limitations imposed by the intrinsically low sensitivity.

1.5. D-DNP

1.5.1 Principles of D-DNP

Dissolution dynamic nuclear polarization (D-DNP) is a hyperpolarization technique capable of providing signal enhancement by creating a high electron polarization at low temperature and transferring it to nuclear spins via hyperfine interactions. Different mechanisms have been introduced to explain the DNP phenomenon, including the Overhauser effect, solid effect, cross effect, and thermal mixing.[55–57] The Overhauser effect was first proposed in the 1950s for systems with mobile electrons such as conducting solids and liquids. It is the phenomenon in which irradiation of an electron-nucleus system near the single-quantum (SQ) electron paramagnetic resonance (EPR) transition induces the relaxation of formally forbidden zero- (ZQ) and double- quantum (DQ) transitions at a different rate. The ZQ and DQ relaxation redistribute the spin populations through rotational motion in liquids or translational modulation of electrons in conducting solids. ZQ relaxation is the dominant pathway in conducting solids and provides a positive enhancement on the nucleus polarization, whereas DQ relaxation dominates in liquids and produces a negative enhancement. The remaining three mechanisms are responsible for polarization transfer in non-conducting solids such as frozen glassing-forming solvents. The solid effect is a two-spin dynamic mechanism that occurs when microwave irradiation is applied at a frequency $\omega_e \pm \omega_n$, where ω_e and ω_n are the electron and nuclear resonance frequency, respectively. The irradiation allows the nominally forbidden ZQ and DQ transitions to occur, producing an EPR spectrum with a positive and negative enhancement at the frequency of $\omega_e \pm \omega_n$. The hyperfine coupling between electrons and the nucleus produces the mixing of spin states and polarization transfer between electrons and nuclear spins. While the dynamics of the spin system is determined from the time-dependent Hamiltonian in the Overhauser effect, it is treated as a time-independent

perturbation in the solid effect. In the cross effect model, polarization transfer occurs in a system of two unpaired electrons that are dipolar coupled when the frequency separation between these two electrons equals ω_n. Microwave irradiation is applied at the allowed SQ EPR transition. This mechanism requires EPR linewidth δ to be inhomogeneously broadened by *g*-anisotropy and larger than ω_n. However, the cross effect is less common in glassy samples due to the low probability of having two electrons at frequencies separated by ω_n. The cross effect has more widely applications in high-field DNP, as the DNP efficiency by this mechanism scales favorably with the magnetic field due to a broader linewidth. Thermal mixing is a process of energy exchange between the electronic non-Zeeman and nuclear Zeeman reservoirs when $\delta \geq \omega_n$. The electron spin ensemble, when interacting with the nuclear spin, produces a homogeneously broadened EPR linewidth. Most DNP techniques fall into the category of continuous wave (CW) DNP, wherein only microwave fields are treated as time-dependent harmonic perturbations, while the remaining Hamiltonian terms are static. In time-domain DNP, time-dependent perturbations from magnetic fields can be introduced by several different means, such as rotating nuclear or microwave frames, matching the electron rotating frame and the nuclear laboratory frame, or sweeping across a magnetic field.

1.5.2. D-DNP Experiments

Polarization of electrons is created at a low temperature in an insert filled with liquid helium. As shown in Figure 1.2, the polarization level of electrons at ~ 1.4 K is 10^4 – 10^5 times higher than that of a common nucleus such as ^{1}H and ^{13}C at room temperature. This difference can be exploited to provide signal enhancement of several orders of magnitude by polarizing the sample at a temperature near zero Kelvin then rapidly dissolving the frozen sample with hot solvent before NMR acquisition takes place in the liquid state near a physiological temperature.

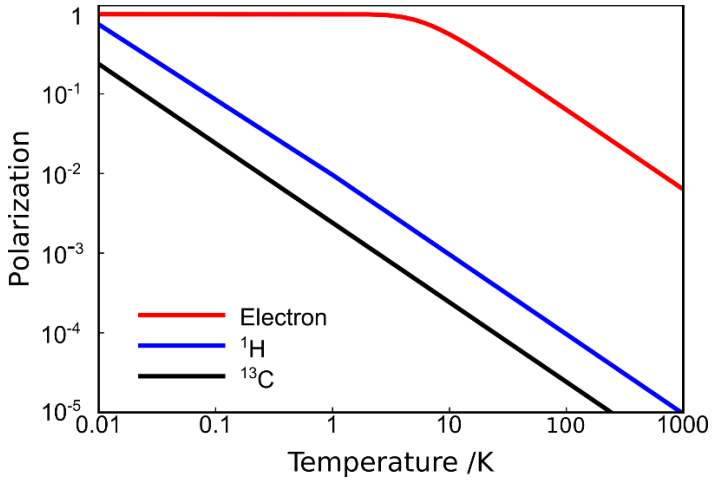

Figure 1.2 Temperature dependence of polarization for electrons, ^{1}H, and ^{13}C nucleus. Microwave irradiation facilitates the polarization transfer from electrons to nuclear spins, resulting in hyperpolarized nuclear spins.

A sample used in D-DNP hyperpolarization typically consists of an analyte that contains the nucleus to be hyperpolarized, a radical that provides the unpaired electrons, and a glassing matrix that freezes at low temperature but allows the sample to be in the liquid phase near room temperature. The T_1 relaxation of the analyte is an important factor of consideration, as it dictates the rate of hyperpolarization decay and the polarization available at the time of NMR measurements. Molecules of smaller sizes (< 300 kDa) typically have higher signal enhancement and a longer T_1, causing hyperpolarization decay over the course of a few seconds. Nitroxyl-based radicals are often used for ^{1}H and ^{19}F polarization, among which 4-hydroxy-2,2,6,6-tetramethylpiperidine-1-oxyl (TEMPOL) is common.[58] The combination of D_2O/dimethyl sulfoxide-d6 (DMSO-d6), D_2O/glycerol-d8, and D_2O/ethanol-d6 are frequently selected as a glassing matrix for preparing sample with TEMPOL.

The general procedures in a D-DNP experiment typically involve the following steps: sample polarization, dissolution, sample injection and mixing, and NMR acquisition. An illustration of the DNP setup is shown in Figure 1.3.

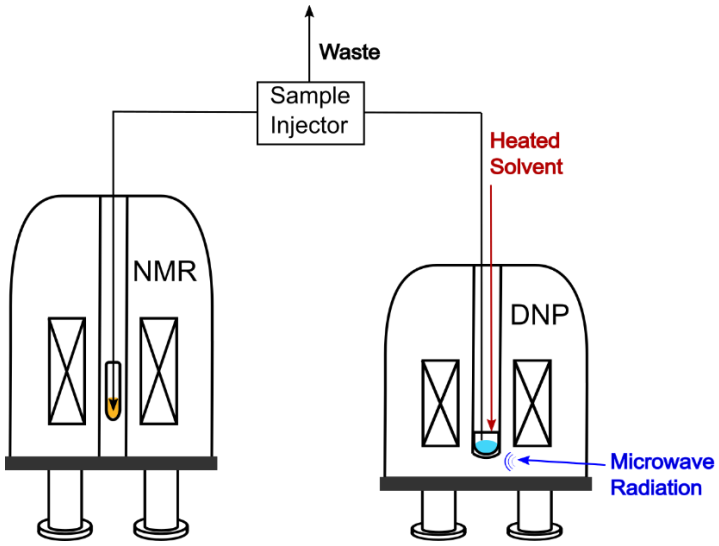

Figure 1.3 Instrumentation for a D-DNP experiment. The DNP sample is first irradiated with a microwave source to create hyperpolarization, followed by sample dissolution with heated solvent. A portion of the dissolved sample is rapidly transferred by a sample injector into an NMR tube preloaded with the non-hyperpolarized sample. The excess sample that is not injected flows to the waste. After a short period of stabilization time, the injection program delivers an electric trigger signal to the NMR program for signal acquisition.

For sample polarization, a 0.1 – 100 μL aliquot of the DNP sample is loaded into a DNP polarizer and irradiated with microwaves of a power and frequency suitable for the nucleus of interest. The optimal frequency can be determined by sweeping across a range of microwave frequencies in the solid state. The polarization time required depends on the type of nucleus, which is generally 20 – 30 minutes for ^{1}H and ^{19}F experiments and a few hours for ^{13}C experiments. A polarization buildup curve can be measured to optimize the polarization time.

For dissolution, the heated buffer is transferred by an automated dissolution system to dissolve the frozen sample. To preserve hyperpolarization, the dissolved sample needs to be injected into the NMR tube situated inside the magnet as quickly as possible. A rapid injection

system capable of sample delivery within a few hundred milliseconds is essential for experiments with ^{1}H and ^{19}F nuclei due to their short T_1 of a few seconds. For protein-ligand binding studies, the hyperpolarized ligand is typically mixed with a non-hyperpolarized sample that contains protein. To ensure the reproductivity and accuracy of the measurements, the sample mixing needs to be homogeneous.

There are different types of injection methods. Gas-driven injectors drive the liquid transfer with a pressurized inert gas such as N_2.[59] For a preloaded volume of 20 – 50 μL protein, the dilution is about 10 – 20 times, considering the typical sample volume of ~ 450 μL for a 5 mm NMR tube. Liquid-driven injectors use water pressure created by syringe pumps to drive the sample.[60] Liquid-driven injectors are more commonly used for applications in need of flow NMR. Prior to the sample transfer, an NMR pulse program is initiated to wait for a trigger from the injection system. A stabilization time of a few hundred milliseconds is typically added to the injection program for the injected sample to stabilize and reach equilibrium, while not causing a significant loss of polarization.

CHAPTER 2

^{1}H RELAXATION-BASED SCREENING OF HIGH-AFFINITY LIGANDS THROUGH COMPETITIVE BINDING

2.1. Introduction

The advent of high-throughput screening (HTS) has led to the discovery of numerous marketed drugs over the past three decades. HTS makes use of automated procedures to screen through compound libraries and identify potential "hits", drug candidates that demonstrate the ability to modulate activities in a biological system of interest and have value for further lead optimization.[61–63] Nuclear Magnetic Resonance (NMR) spectroscopy has emerged as a powerful HTS tool owing to its distinct capability of providing reliable information about the binding kinetics and thermodynamic parameters with less chance of producing artifacts compared to other commonly used techniques. Ligand-observed NMR, which operates based on observation of ligands rather than targeted macromolecules, is well suited for the purpose of HTS. It has been shown effective for detecting binding of low- and medium-affinity ligands to proteins of various sizes at a micromolar concentration.[64,65] However, its inadequacy in detecting strong binders severely limits its utility for drug discovery, as high-affinity ligands are often potent drug candidates. The problem arises from the slow exchange experienced by strong binders with a dissociation constant (K_D) in the nanomolar regime.[11] In this case, the exchange rate is smaller than the difference in chemical shift between the free and bound states of a ligand, giving rise to a separate signal for each state. With a slow rate of dissociation, merely a small fraction of the ligands binds and readily saturates the binding sites, while the majority maintains the relaxation properties of the free form. This disparity causes the signal change due to protein-ligand interactions to be minimal, precluding direct detection of the binding.

The use of competitive binding has been previously introduced to compensate for this drawback and has shown success in detecting high-affinity ligands.[31] The concept of competitive binding has been incorporated to observe binding with various types of ligand-observed NMR methods such as ^{1}H and ^{19}F relaxation methods,[31,66,67] saturation transfer difference (STD) spectroscopy,[68] and water-ligand observed via gradient spectroscopy (water-LOGSY)[69]. Competitive binding experiments involve a ligand of interest competing against a low- to medium-affinity reporter ligand of known K_D. Through changes in the transverse relaxation rate (R_2) of the reporter ligand, it is possible to indirectly probe the interaction between a ligand of interest and the protein target and to derive an estimation of K_D for the competing ligand. The relaxation rate of the reporter ligand at the competitive equilibrium ($R_{2,c}$) is in-between those of free reporter ligand ($R_{2,f}$) and bound reporter ligand without competition ($R_{2,b}$).[67] The use of competitive binding is advantageous in several different ways. Competitive binding enables the detection of high-affinity drug candidates that commonly produce false negative identification of binding by other ligand-observed NMR methods. The binding interaction detected by competitive binding is also specific to the active site and avoids the contribution from nonspecific binding or allosteric inhibition.[31]

Dissolution Dynamic Nuclear Polarization (D-DNP)[54] can provide a signal enhancement of several orders of magnitude by creating a non-Boltzmann distribution of spin states. The incorporation of D-DNP has significantly improved the sensitivity of ligand-observed NMR to detect ligands in the low-micromolar regime and advanced its practicability for drug screening. Initial applications of hyperpolarized NMR in parallel with competitive binding have been realized for hyperpolarized long-live spin states.[70] The subsequent development has enabled screening

ligands of various binding affinities and determination of K_D in a single scan through detection of ^{19}F NMR signals without titrations.[67] Hyperpolarization of ^{1}H nuclei for detecting competitive binding has been demonstrated for other types of ligand-observed methods such as water-LOGSY.[71] A challenge of ^{1}H-based detection lies in the large signal interference from water protons that overlaps and masks the desired ligand signal, which is generally broad and less resolved in R_2 experiments.

Here, a novel ligand-observed NMR method that allows ^{1}H detection of strong binding interactions through R_2 change was developed by applying competitive binding in conjunction with D-DNP. The development of such a detection method for the ^{1}H nucleus will diversify the ligand pool that can be detected, considering most compounds contain protons. The interaction between 2',3'-cyclic-GMP-AMP (2',3'-cGAMP) and stimulator of interferon (STING) investigated in this study are promising targets for cancer immunotherapy.[72] The interaction between 2',3'-cGAMP and STING plays a central role in the cGAS-STING pathway that mediates innate immune antiviral and antitumor response.[72–74]

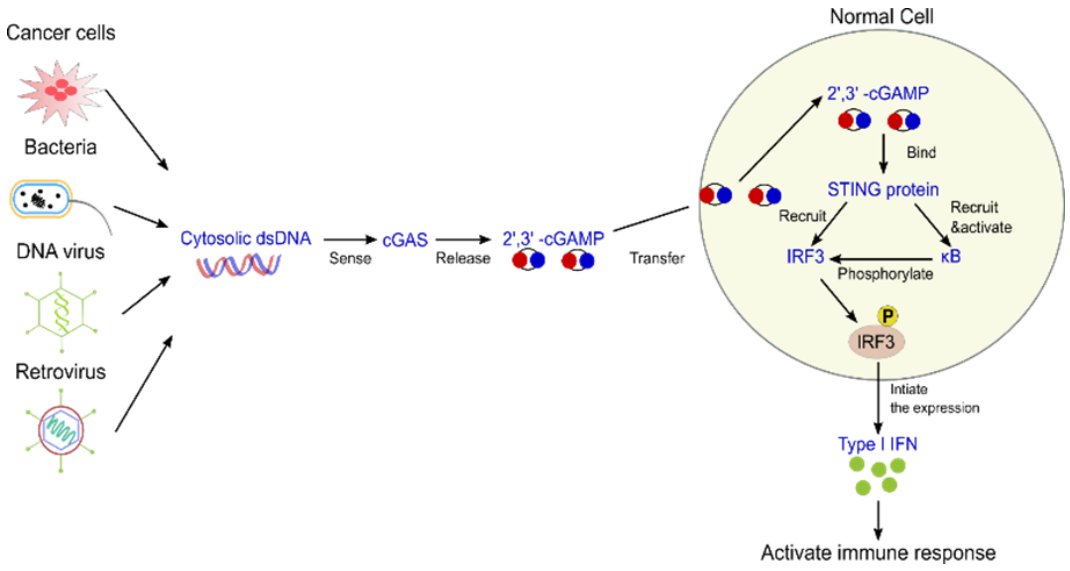

Figure 2.1 The cGAS-STING pathway and its role in primary host immune responses. The sensing of cytosolic dsDNA by cGAS triggers the release of 2',3'-cGAMP, which binds to the STING protein to facilitate the production of Type-I IFN and activate innate immune responses.

In the cGAS-STING pathway, the secondary messenger, cyclic GMP-AMP synthase (cGAS), activates upon sensing cytosolic dsDNA and catalyzes the release of 2',3'-cGAMP. Binding of 2',3'-cGAMP to adaptor protein STING triggers a series of downstream regulations that stimulates the production of Type-I interferon (IFN), which promotes the expression of antiviral proteins and induces responses of antitumor T-cells and Natural Killer (NK) cells. STING is an innate immune sensor of cyclic dinucleotides, which contains four transmembrane helices localized on the endoplasmic reticulum membrane and a cytoplasmic ligand-binding C-terminal domain (CTD). 2',3'-cGAMP is a high-affinity agonist of STING CTD (K_D ~ 3.79 nM)[75] that putatively competes against a medium-affinity reporter ligand, cyclic di-GMP (cdG) (K_D ~ 1.21 μM).[76]

2.2. Experimental Methods

The protein STING CTD (10 mg/mL) and competing ligand 2',3'-cGAMP samples were preparing using previously described methods[72,77] and provided by our collaborator. The identity of 2',3'-cGAMP was verified with ^{1}H NMR spectroscopy and electrospray ionization mass spectrometry (ESI-MS). For D-DNP experiments, the sample for hyperpolarization was prepared by dissolving 20 mM cyclic di-GMP (cdG) (InvivoGen, San Diego, CA) in D_2O: d_6-DMSO (1:1 v/v; Cambridge Isotope Laboratories, Tewksbury, MA) containing 15 mM 4-hydroxy-2,2,6,6-tetramethylpiperidine-1-oxyl (TEMPOL) radicals (Sigma Aldrich, St. Louis). To create ^{1}H hyperpolarization, an aliquot of this DNP sample (1-10 µL) was loaded into a HyperSense DNP polarizer (Oxford Instruments, Abingdon, UK) and irradiated with a 100 mW of 94.005 GHz microwave at 1.4 K for ~ 30 minutes. Meanwhile, a 5 mm NMR tube was preloaded with the non-hyperpolarized sample prepared in D_2O buffer at pH = 8.0. The D_2O buffer recipes included buffer 1 (50 mM Na_2HPO_4 /NaH_2PO_4), 2 (50 mM K_2HPO_4 /KH_2PO_4), and 3 (20 mM Na_2HPO_4 /NaH_2PO_4, 150 mM NaCl). For free ligand experiments, the preloaded sample was either absent or only contained buffer. For bound ligand experiments, STING CTD was preloaded with or without buffer. For competitive binding experiments, a mixture of STING CTD and 2',3'-cGAMP (10 mM) was preloaded with or without buffer. After polarization, the frozen sample was dissolved with heated D_2O buffer (4 mL) at 10 bar. Using a previously described gas-driven injector,[59] the dissolved sample was rapidly transferred (within 380-400 ms) into the preloaded NMR tube situated inside a 400 MHz NMR spectrometer (Bruker Biospin, Billerica, MA) equipped with a Triple Resonance Inverse (TXI) probe. The injected sample was allowed to stabilize for 500 ms before the pulse program initiated. The pulse sequence used for the CPMG experiments is illustrated in Figure 2.2. Single-scan CPMG modules were used for data acquisition after solvent

suppression and selective excitation of the ligand aromatic protons at 8 ppm. In most experiments, an optional continuous wave (CW) pulse was applied to suppress the DMSO signal. For water suppression, three cycles of pulsed-field gradients were applied on the water resonance. Data collected for the CPMG experiments were analyzed with Python (Python Software Foundation, Fredericksburg, VA) by applying a sine-shape window function and a phase correction to maximize the real and minimize the imaginary part of the CPMG echoes. A single exponential function was fitted to the real part to obtain R_2 values.

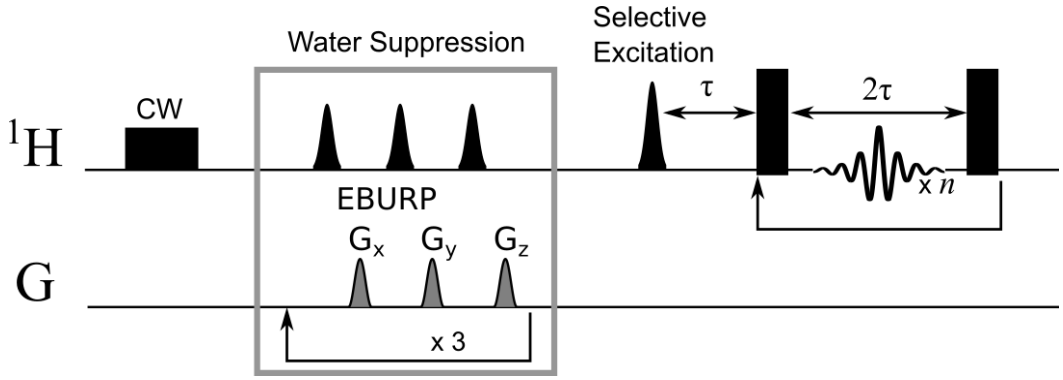

Figure 2.2 Single-scan CPMG pulse sequence used for ^{1}H hyperpolarized experiments measuring R_2. The application of an optional CW pulse allowed the suppression of the DMSO resonance. Pulsed-field gradients, consisting of three 90˚ EBURP pulses and three gradients in the *x*, *y*, and *z* directions, were applied three times to suppress the water signal. This was followed by a 90˚ EBURP pulse to selectively excite ligand aromatic protons. Acquisition of spin echoes for determination of R_2 was accomplished with a CPMG module.

The signal enhancement of cdG was evaluated prior to the hyperpolarized CPMG experiments. A ^{1}H hyperpolarized NMR spectrum of cdG was acquired after water suppression and compared to a non-hyperpolarized spectrum acquired after hyperpolarization decay. The final concentration of cdG in each injected sample was determined by comparing its aromatic proton signal in a water-suppressed non-hyperpolarized spectrum measured after injection to that in a water-suppressed reference spectrum of 200 μM cdG in 99.5% D_2O (100x dilution of the DNP sample). Final

concentrations of STING CTD and 2',3'-cGAMP were quantified from averages of dilution factors from several injection tests, where reference compounds of the same initial volume as the preloaded components were loaded, and the concentration difference of each reference compound before and after the injection was used to determine the dilution factors.

Control experiments used nearly identical conditions as the D-DNP competitive binding experiments to directly probe the binding of 2',3'-cGAMP to STING CTD. The sample used for hyperpolarization was replaced with 5 μL of 20 mM 2',3'-cGAMP, which was directly polarized and dissolved with buffer 1 prior to its injection into a preloaded NMR tube in the presence versus absence of 20 μL STING CTD.

2.3. Results and Discussion

Competition experiments were applied with D-DNP to detect binding of a high-affinity ligand 2',3'-cGAMP to the STING CTD through changes in R_2 of a hyperpolarized reporter ligand cdG. Binding of competing ligand causes changes in the fraction of bound reporter ligands and results in perturbations on the R_2 of the latter. Hyperpolarization of cdG was first performed to determine its ^{1}H signal enhancement and evaluate the feasibility of using it as a reporter ligand in hyperpolarized R_2 experiments. Figure 2.3. shows the acquired ^{1}H hyperpolarized spectrum of cdG, along with a structural illustration of this symmetrical molecule. A signal enhancement of 1367 and 1285 was achieved for the signal from the two equivalent aromatic protons (H_a) on the GMP moieties near 8.0 ppm and the signal from the anomeric protons (H_b) near 6.0 ppm, respectively. The aromatic protons were chosen as the target for observation because they appear far from the water resonance at 4.7 ppm, the region to which water suppression should be applied.

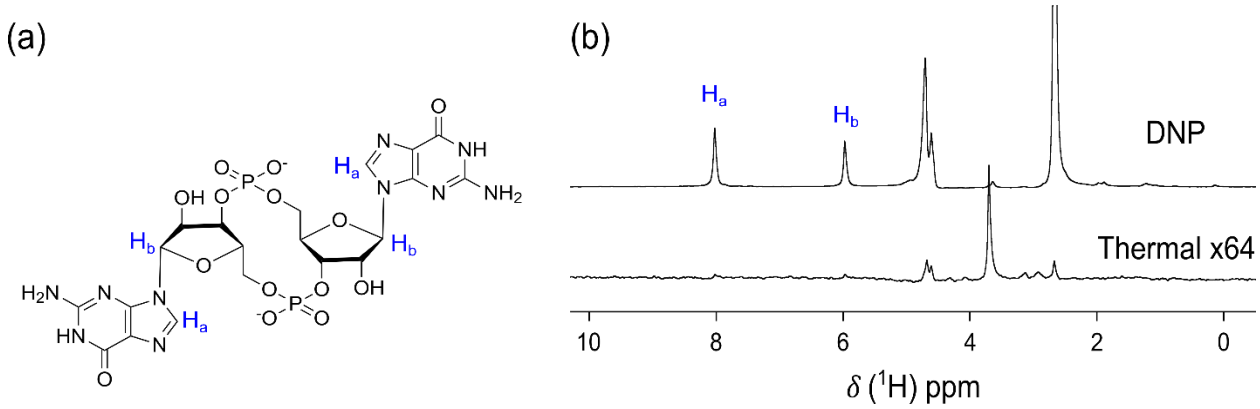

Figure 2.3 Characterization of cdG. Chemical structure of cdG (b) ^{1}H water-suppressed spectrum of DNP hyperpolarized cdG in D_2O sodium phosphate buffer. Chemical shift assignments for H_a and H_b are indicated.

Single-scan CPMG experiments were performed to observe the R_2 of hyperpolarized cdG in the absence and presence of STING CTD without competition as well as in the presence of protein under competition. Selective excitation was applied at 8 ppm for observing H_a after water suppression. Figure 2.4 shows the acquired initial CPMG echoes of free cdG polarized at varying volumes to illustrate the achievable resolution for the signal from the ligand aromatic protons. Hyperpolarization with D-DNP resulted in an enhanced CPMG echo intensity near 8 ppm. The excited ligand signal was separately observable from the suppressed water signal at a concentration as low as 36 µM with a 1 µL cdG aliquot polarized and became well resolved at >50 µM when polarizing aliquots of 2 µL or more.

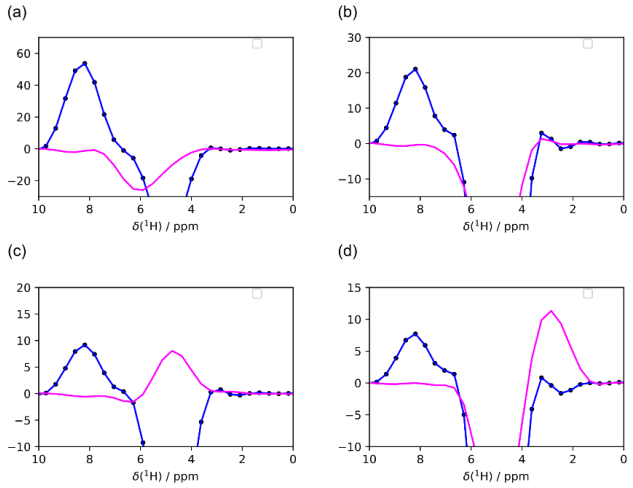

Figure 2.4 Spectra of the first CPMG echo illustrating the achievable resolution for the signal from the cdG equivalent aromatic protons H_a (8 ppm). These spectra were acquired for a varying amount of DNP polarized cdGs (a) 205 µM (10 µL polarized), (b) 146 µM (5 µL polarized), (c) 51 µM (2 µL polarized), and (d) 36 µM (1 µL polarized).

The CPMG echo intensities were monitored over time and integrated. The integrated intensities were fitted with an exponential function to construct curves for determination of R_2. Figure 2.5 (a) shows the acquired CPMG echo intensities as a function of time for experiments with 10 µL of polarized cdG. The decay of the H_a signal over time is seen in the diminishing magnitude of CPMG echo intensities. The fitted R_2 curves with the integrated CPMG echo intensities over a course of 10 s are shown in Figure 2.5 (b). Measurements with the free reporter ligand and reporter in the presence of protein without competition are indicated as the free and bound experiment, respectively, which were used to determine the corresponding relaxation rates $R_{2,f}$ and $R_{2,b}$. Those with the reporter in the presence of protein under competition are referred to as the competitive binding experiment, from which the $R_{2,c}$ values were determined.

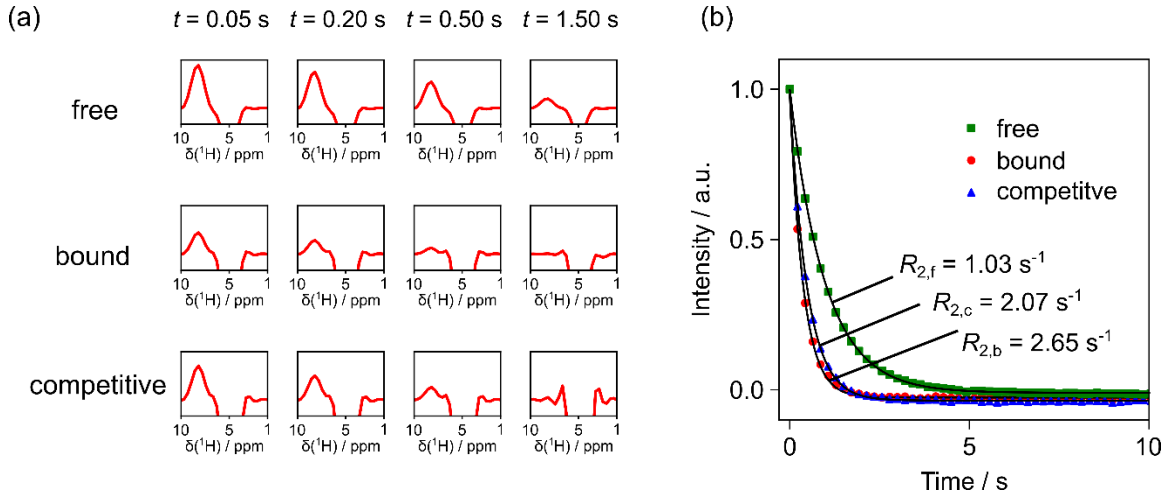

Figure 2.5 Hyperpolarized R_2 experiments with 10 µL polarized cdG. (a) Selected spectra of CPMG spin-echoes obtained after solvent suppression and selective excitation of cdG aromatic protons H_a for the free, bound, and competitive binding experiment (b) integrated CPMG spin-echo intensities and fitted R_2 curves for the free (■), bound (●), and competitive binding measurements(▲). Preloaded samples used in each of these experiments were 30 µL buffer, 20 µL 10 mg/mL STING CTD with 10 µL buffer, and 20 µL STING CTD with 10 µL of 10 mM 2',3'-cGAMP, respectively. Data shown here were acquired using buffer 3, an injection time of 380 ms, and CW pulse.

The experiment with 10 µL cdG resulted in an $R_{2,f} = 1.03\ s^{-1}$ that falls within the typical R_2 range of small molecules. The addition of 20 µL STING CTD produced a larger $R_{2,b} = 2.65\ s^{-1}$, an increase of 157%. This observation aligns with the anticipation that ligands in the bound complex exhibit a longer rotational correlation time (τ_c) and produce a faster transverse relaxation corresponding to the behavior of macromolecules. Competitive binding experiments are anticipated to result in curves that lie in between those from the free and bound experiment. The observed curve with the addition of 10 µL 2',3'-cGAMP was in-between but closer to the curve from the bound experiment, yielding an $R_{2,c} = 2.07\ s^{-1}$. Similar observations were also reflected in different rates of decay for the H_a signal as illustrated by Figure 2.5 (a). The decay was the fastest in the free experiment, the slowest in the bound experiment, and in-between in the competitive

binding experiment. These changes in the signal decay and R_2 might be indicative of competition and displacement of cdG by bound 2',3'-cGAMP molecules. However, the occurrence of competition cannot be concluded from this observation, as the observed curve in the competitive binding experiment was close to the curve in the bound experiment. Although standard errors from R_2 fitting computed for all three experiments were less than 0.4%, additional experiments are necessary to account for experimental errors due to variations in concentrations.

To optimize the experimental conditions, attempts were made to reduce the required concentrations of ligand and protein counterparts. Experiments with 5 µL cdG polarized yielded an average $R_{2,f} = 0.96 \pm 0.07\ s^{-1}$, consistent with the finding described in Figure 2.6 for 10 µL cdG. When the amount of polarized cdG was further reduced to 2 µL, a faster average relaxation of $R_{2,f} = 1.81 \pm 0.32\ s^{-1}$ was observed instead. This difference might be explained by an increasing influence from residual water resonance at a lower ligand concentration. A positive correlation between the amount of preloaded protein and $R_{2,b}$ was observed as expected due to an increase in the fraction of bound reporter ligand. For bound ligand experiments with 5 µL cdG, the observed $R_{2,b}$ increased from 1.55 ± 0.04 to $2.14 \pm 0.11\ s^{-1}$ upon doubling the amount of preloaded STING CTD (10 mg/mL) from 10 to 20 µL. A similar observation was made for experiments with 2 µL cdG. The average $R_{2,b}$ was $2.85 \pm 0.32\ s^{-1}$ in the presence of 6 µL STING CTD (2.5 mg/mL). The ligand signal became over-broadened when the amount of preloaded STING CTD was increased to 15 µL. The observation made for $R_{2,c}$ when 5 or 2 µL cdG was polarized, however, appears to be contradictory to the result for 10 µL cdG. Competitive binding experiments with 5 µL cdG suggest that relaxation became faster compared to $R_{2,b}$ in the presence of 2',3'-cGAMP, and $R_{2,c}$ became larger as the amount of added 2',3'-cGAMP (10 mM) increased ($R_{2,c}$ = 1.82, 1.95, and

1.99 s^{-1} for 2, 5, and 10 µL 2’,3’-cGAMP). The result from competitive binding experiments with 2 µL cdG also produced a larger $R_{2,c}$ in all instances, but no correlation between a faster relaxation and increasing amount of 2’,3’-cGAMP was observed. These unexpectedly large $R_{2,c}$ might indicate allosteric effect or be attributed to the interference from water resonance at low ligand concentrations.

To validate the necessity of using competitive binding, control experiments were performed by attempting to directly probe the binding between 2’,3’-cGAMP and STING CTD. The acquired CPMG echoes for the control experiments are shown in Figures 2.6 (a), suggesting no obvious change in the signal intensity for echoes obtained from experiments in the absence versus presence of 20 µL STING CTD. The integrated intensities of these echoes and the fitted R_2 curves are displayed in Figure 2.6 (b). The resulted R_2 of 0.75 and 0.73 s^{-1} corresponding to the free and bound experiments also reflects a lack of change due to binding. The strong binding interaction between 2’,3’-cGAMP and STING CTD escaped detection and produced a false negative when direct observation was attempted. This is expected due to the saturation of binding sites by a small fraction of 2’,3’-cGAMP, while most of the ligand remains in the free form.

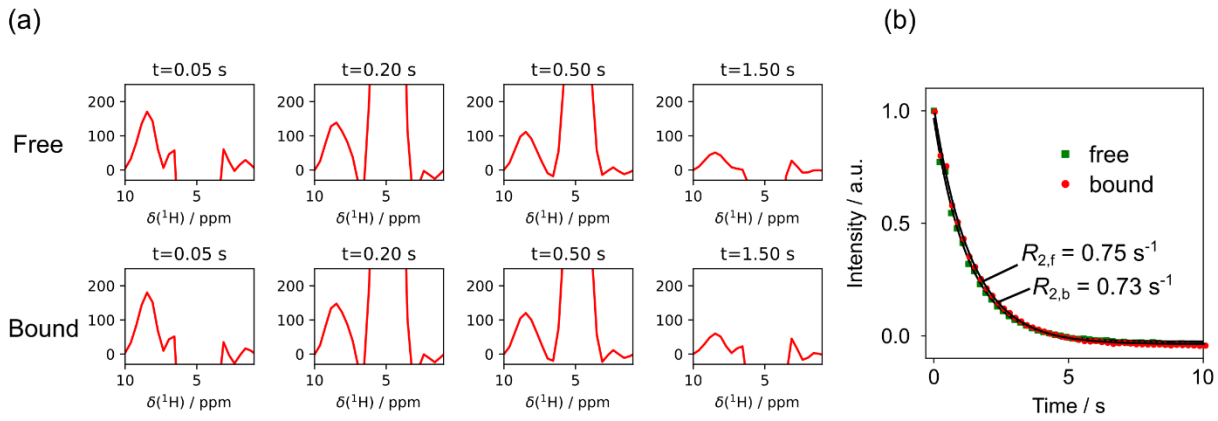

Figure 2.6 Hyperpolarized R_2 control experiments with 2',3'-cGAMP. (a) Selected spectra of CPMG spin-echoes obtained after solvent suppression and selective excitation of 2',3'-cGAMP aromatic protons (~ 260 µM) for the free and bound ligand experiments (b) CPMG spin-echo intensities and fitted R_2 curves in the absence (■) versus presence (●) of 40 µL 10 mg/mL STING CTD. Data shown here were acquired using H_2O as dissolution buffer, an injection time of 400 ms, and no CW pulse.

The final concentration of cdG after each experiment was quantified by comparing its non-hyperpolarized spectrum after injection to a reference spectrum. Following this method, an average cdG concentration of 227 µM was obtained for data shown in Figure 2.6, agreeing with [cdG] = 228 µM determined from the dilution factor (88x) for a polarized volume of 10 µL. Final concentrations of 2',3'-cGAMP (33x dilution) and STING CTD (17x dilution) characterized from dilution factors were 302 and 22.8 µM, respectively.

Additionally, characterization of the competing ligand 2',3'-cGAMP was performed with ^{1}H NMR spectroscopy and ESI-MS to verify the identity of the compound. The ^{1}H NMR spectrum of 2',3'-cGAMP in D_2O was measured after water suppression and is displayed in Figure 2.7. The measured chemical shifts closely resemble the values in a previously reported spectrum.[76] The signals near 8.4 and 8.0 ppm are attributed to the two aromatic protons on the adenosine monophosphate (AMP) and guanosine monophosphate (GMP) moieties (H8) and a single aromatic

proton on the GMP moiety (H2). Signals near 6.0 ppm are from the anomeric protons on the two deoxyribose moieties. The ESI-MS measurement of 2',3'-cGAMP sodium salt ($[M-H]^-$), shown in Figure 2.7, indicates a molecular weight of 673.09 kDa, similar to a published value of 675.11 kDa from a Tandem-MS measurement ($[M+H]^+$).[76]

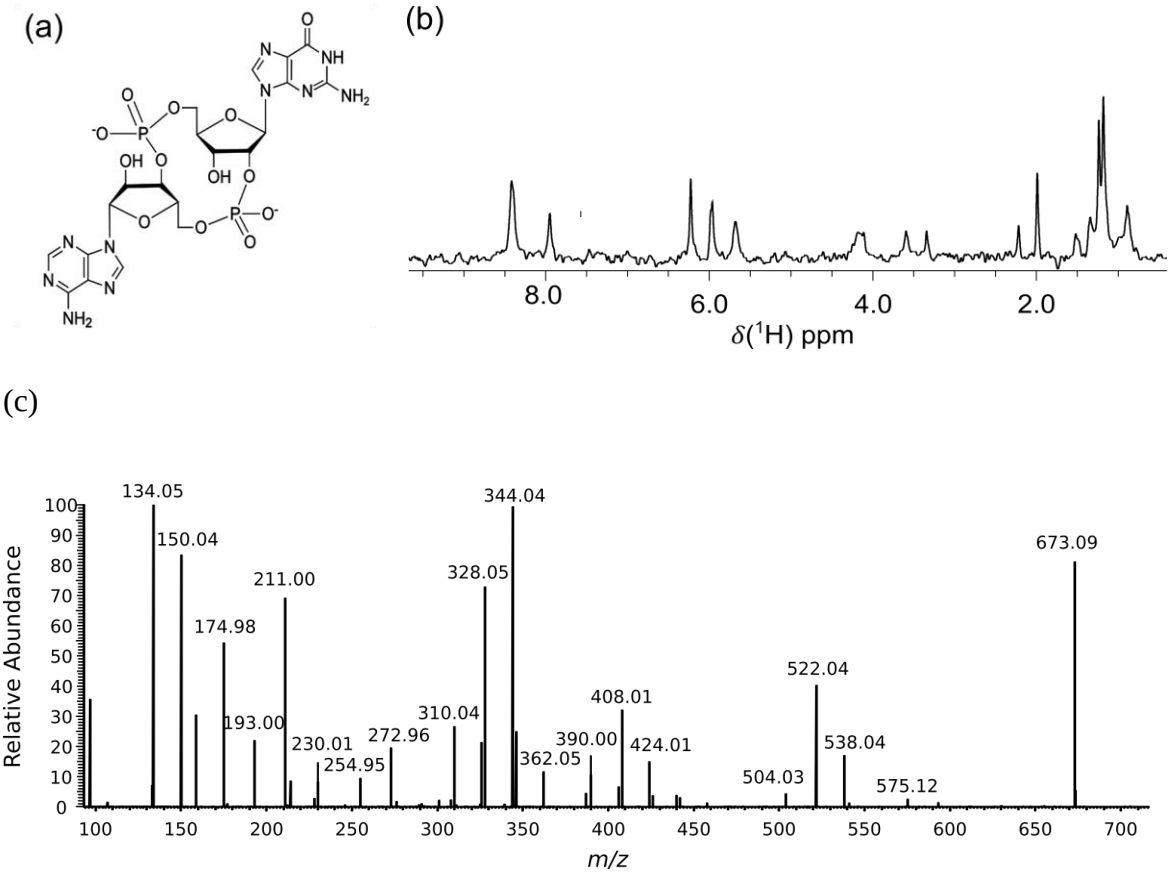

Figure 2.7 Characterization of 2',3'-cGAMP. (a) Chemical structure of 2',3'-cGAMP (b)^{1}H NMR spectrum of 2',3'-cGAMP in D_2O (c) ESI-MS spectrum of 2',3'-cGAMP sodium salt ($[M-H]^-$) indicating a mass of 673.09 kDa.

While D-DNP methods exist for the detection of strong binding through heteronuclear observation of R_2 change, ^{1}H-based observation could be challenged by the presence of a large water signal that overlaps and interferes with the ligand resonance. The use of D-DNP enhanced

the ligand signal by >1000x to an observable magnitude compared to the water signal, allowing the detection of ligands in the low micromolar concentration regime. In this study, several additional strategies have been adopted to overcome this challenge. First, deuterated solvent was used in both sample preparation and dissolution to minimize the amount of water introduced. Second, selective excitation was performed on the aromatic protons of the reporter ligand near 8 ppm, while most water protons remained off-resonance and unexcited. The aromatic protons were selected because their chemical shifts are generally farther away from that other types of protons, and they typically exhibit a long spin-lattice relaxation time (T_1). Attempts have been made to excite the anomeric protons near 6 ppm but yielded a poorly resolved signal that overlapped with the water resonance. Third, pulsed-field gradients were applied to dephase the water coherence and further suppress the water signal. This technique was still necessary despite the use of deuterated buffer and selective excitation. The inevitable presence of proton residuals in any deuterated solvent still creates a relatively large, undesirable water signal from hyperpolarization. The selective excitation of ligand signals can generate a small amount of excitation on the unwanted water resonance. We demonstrate here that the employment of these strategies has effectively reduced the interference from the water signal for the ligand signal to be resolved using D-DNP. Results from characterization of $R_{2,c}$, however, remain inconclusive and require further work. In the future, subtraction of water background could be adopted as a strategy to reduce the effect of water signal if the observed water signal for each echo is similar among measurements.[78] Nevertheless, the development of this ^{1}H-based provides a means of detecting ligands at a wide range of affinities with single-scan D-DNP experiments. The observation of ^{1}H spins enlarges the pool of ligands available for screening by D-DNP, considering that most ligands contain protons.

2.4. Conclusions

In summary, a ^{1}H relaxation-based screening method has been developed to probe strong protein-ligand binding using D-DNP. Competitive binding was used to compensate for the inadequacy of ligand-observed methods in detecting high-affinity ligands. Hyperpolarization created by D-DNP provided a thousandfold signal enhancement, allowing detection at a protein concentration in the low micromolar regime. A faster relaxation of the reporter ligand was observed at various concentrations upon its binding to the protein target. The effect of adding the putative competing ligand on R_2 remains inconclusive. The challenge of ^{1}H-based detection originated from a larger water proton signal was overcome with the use of solvent suppression and selective excitation, resulting in a resolved signal from ligand ^{1}H spins. The observation of the ^{1}H nucleus makes the D-DNP method compatible with the observation of most small-molecular reporter ligands.

CHAPTER 3

^{19}F NOE-BASED SCREENING FOR QUANTIFYING BINDING WITH HYPERPOLARIZED WATER

3.1. Introduction

The dynamic interaction between proteins and small molecules plays a central role in mediating a diversity of fundamental biological processes such as signal transduction, enzymatic catalysis, and stimulation of immune responses.[1] Characterization of protein-ligand interactions is at the core of drug discovery as well as understanding of relevant biological functions that are vital to life. Nuclear Magnetic Resonance (NMR) has emerged as a powerful, nondestructive tool for studying the kinetics and dynamics of protein-ligand interactions, with a prominent advantage in characterizing weak interactions when compared to other techniques.[11] Transfer of water polarization is a sensitive ligand-observed NMR approach capable of characterizing biomolecular interactions such as interactions of small molecules and proteins with water.[49,65,69] It can also provide characterization of protein-ligand interactions with the unique ability to identify false positive signals caused by protein aggregation.[65] Detection of protein-ligand interactions based on transfer of water polarization may exploit either of the two pathways, via the exchange of labile protons (NH and OH) or via the nuclear Overhauser effect (NOE).[11] Water polarization can be transferred to the exchanging protons of a small molecule through chemical exchange. Transfer of water polarization can also be achieved through NOE, which originates from the dipole-dipole cross relaxation.

A limitation of this method is that the acquired signal intensity is typically a magnitude or two weaker than that that of the original signal in most experiments, as only the transferred

magnetization is detected.[71] By creating a highly nonequilibrium nuclear spin state of water protons, hyperpolarization can indirectly enhance transfer of polarization through proton exchange or the cross-relaxation process. D-DNP is capable of consistently creating a ^{1}H polarization in excess of 5% or more for samples of 2-6% H_2O in D_2O, resulting in a water signal of 10-100x stronger than pure water in conventional NMR.[79] The use of D_2O can prolong the longitudinal relaxation (T_1) of water protons by several fold up to a time of 40 s.[80] Recent implementations of hyperpolarized water in our research group have enabled the observation of transient ^{19}F signal enhancement of small fluorinated molecules[42] as well as kinetic modeling of water magnetization transfer to proteins.[81] Using hyperpolarized water, Frydman and coworkers have achieved hundredfold ^{15}N signal enhancement for small molecules through heteronuclear NOE with exchangeable amine or amide protons.[80] Further optimization of water polarization (≥20%) has led to 1D and 2D biomolecular NMR experiments that feature ≥300x sensitivity enhancement compared to their non-hyperpolarized counterparts.[80] More recently, hyperpolarized water has enabled the resolution of site-specific signal enhancements for individual amino acid residues in ^{1}H-^{15}N HMQC experiments.[82]

Hyperpolarized water can be applied to characterize protein-ligand interactions through magnetization transfer to ligand spins. In conventional NMR, Water-LOGSY (water-ligand observed via gradient spectroscopy), first demonstrated by Dalvit *et al*., is a classic ligand-based NMR approach that utilizes transfer of water polarization to characterize weak-to-medium binding. The first method that utilizes hyperpolarized water to detect protein-ligand binding, known as DNP-water-LOSGY, was developed by Chappius *et al*, and has enabled ^{1}H-based detection of weak binding through direct observation and strong binding through competition experiments.[71]

The use of hyperpolarized water to probe protein-ligand interaction is advantageous in a number of ways. Compared to direct hyperpolarization of ligands, hyperpolarization of water is more robust and reproducible. The former requires fast protein-ligand association after rapid injection of the hyperpolarized ligand in several hundred milliseconds before the decay of hyperpolarization, which prevents ligands of short T_1 or slow protein-ligand equilibria to be detected. The use of hyperpolarized water as a universal polarizing contrast agent expands the scope of ligands that can be studied and provides a means to probe slow kinetics by allowing for premixing of protein and ligand.

^{19}F-based detection is highly applicable to drug screening, considering that 20% of marketed drugs contain fluorine.[83] Heteronuclear observation of ^{19}F also has the advantage of high sensitivity and specificity, given the 100% natural abundance of ^{19}F. Direct hyperpolarization of ^{19}F spins has been employed in most current studies for characterizing the binding of fluorinated ligands to a protein. Detection of interactions between fluorinated small molecules and proteins at sub-micromolar concentrations were demonstrated for ligands of various affinities through the D-DNP enhanced relaxation experiments.[60,67,83] Inspired by the water-LOGSY experiment, a high-throughput ^{19}F-based method that detects binding through transfer of D-DNP enhanced water polarization is being developed here. We then show that the difference in the apparent ^{1}H-^{19}F cross-relaxation rates (σ) of a fluorinated ligand upon binding can serve as a quantitative measure for binding. Small molecules such as ligands exhibit a short rotational correlation time (τ_c) and acquire a negative NOE enhancement that corresponds to a positive cross-relaxation rate. Upon binding, ligands in the bound complex experience a slower tumbling and longer τ_c that is characteristic of macromolecules, and yield a less negative NOE enhancement and a smaller cross-

relaxation rate. As in the water-LOGSY experiment, transfer of water polarization to ligand spins acquires the protein-mediated pathway in addition to a direct transfer. At last, we demonstrate that the use of a ^{1}H-^{19}F dual-channel homemade spectrometer can provide a real-time characterization of water signal enhancement that affects the accuracy of fitted σ.

3.2. Experimental Methods

The non-hyperpolarized ligand solution was prepared from 4-(trifluoromethyl) benzene-1-carboximidamide (TFBC) (Matrix Scientific, Columbia, SC) in D_2O buffer (50 mM Na_2HPO_4 /NaH_2PO_4, pH = 8.0). Trypsin (Sigma Aldrich, St. Louis, MO) was dissolved using the same buffer to prepare the protein solution. To achieve water hyperpolarization, 100 μL of 1:1 v/v H_2O/DMSO-d6 (Cambridge Isotope Laboratories, Tewksbury, MA) containing 15 mM 4-hydroxy-2,2,6,6-tetramethylpiperidine-1-oxyl (TEMPOL) radicals (Sigma Aldrich) was loaded into a HyperSense DNP polarizer (Oxford Instruments, Abingdon, UK) and irradiated with microwaves (100 mW, 94.005 GHz) at 1.4 K for 30 – 40 minutes. The hyperpolarized sample was dissolved with heated D_2O buffer (50 mM Na_2HPO_4 /NaH_2PO_4, pH = 8.0) at 10 bar and rapidly transferred (within 350 ms) into a 5mm NMR tube using a previously described gas-driven injector.[59] The NMR tube was preloaded in a 9.4 T magnet, where 50 μL of TFBC or mixture of TFBC and trypsin (Sigma Aldrich, St. Louis) was preloaded. The mixture contained 15 mM or 60 mM TFBC in the absence and presence of 900 μM or 1.8 mM trypsin, respectively. The ^{1}H coil of a Broad Band-Observe (BBO) probe (Bruker Biospin, Billerica, MA) was tuned to the ^{19}F frequency, after the shimming and field calibration using ^{1}H. The change in ^{19}F signal intensity for a preloaded sample of 15 mM TFBC in the presence and absence of 900 M trypsin was monitored with a single-channel spectrometer (Bruker Biospin). A series of 45° flip angle pulses was applied to excite the ^{19}F resonance of TFBC

(~63 ppm) over a course of ~29 s (32 scans, 900 ms for each acquisition). The same pulse sequence was applied to measure the transient ^{19}F NOE buildup after injection of hyperpolarized water and after hyperpolarization decay. Single-channel measurements were performed for a preloaded sample of 60 mM TFBC in the presence and absence of 1.8 mM trypsin to demonstrate the effect of ligand-to-protein (L:P) ratio for an injected ligand concentration ranging from 1.5 – 6 mM. ^{1}H hyperpolarized experiments were performed on the same day as the ^{19}F measurements but in separate acquisitions to characterize the water signal enhancement. A 0.1˚ excitation pulse was applied on the water resonance with the probe tuned to the ^{1}H frequency, and the signal intensities of hyperpolarized and non-hyperpolarized water were compared to calculate the water signal enhancement factor. The average water signal enhancement factor from 6–8 measurements was used for fitting the cross-relaxation rates. In all experiments, the final concentrations of water protons and ligand ^{19}F spins were quantified by comparing a ^{1}H/^{19}F thermal spectrum to that of a reference sample at a known concentration. The final concentration of trypsin was calculated based on dilution factors (ζ), which were determined from the concentration difference of TFBC before and after injection. The longitudinal relaxation time (T_1) of both ^{1}H and ^{19}F spins was measured for each injected sample using an inversion-recovery experiment.

To enable real-time measurement of water signal enhancement, a dual-channel spectrometer was constructed to simultaneously measure the ^{1}H and ^{19}F signals using a RadioProcessor (RP), PulseBlaster (PB), and receiver-only RP board (RP-RX) (SpinCore Technologies, Gainesville, FL) based on an earlier design.[42,60] A more detailed description of this spectrometer is included in the Appendix A.1. Both channels were passed through a radiofrequency (RF) combiner/splitter that was connected to the ^{1}H coil of the BBO probe, which

was tuned to the ^{19}F frequency. LabVIEW (NI, Austin, TX) programs were used for controlling the boards and pulse programming. The pulse length of each channel was calibrated by measuring a nutation curve with a sample of 100 mM TFBC in H_2O. The change in ^{19}F signal intensity for a preloaded sample of 60 mM TFBC in the presence versus absence of 1.8 mM trypsin was monitored by applying a series of 50° flip angle pulses to excite the ^{19}F resonance of over a course of ~29 s. A 1° pulse was applied to the ^{1}H channel for measuring the hyperpolarized water signal in real time simultaneous to the ^{19}F acquisition. The hyperpolarized water signal was compared to a non-hyperpolarized signal acquired with a 10° pulse for determining the raw water signal enhancement (ε_{raw}). A calibration curve was measured to evaluate the signal linearity of the ^{1}H channel and to determine the correction factor needed to account for any non-linearity. The resulted correction factor was applied to the raw water signal enhancement to determine the corrected water signal enhancement (ε_{corr}). The method used for constructing the calibration curve is described in Appendix A.2.

Data analysis was performed using Matlab (MathWorks, Natick, MA). An exponential window function was applied to each ^{19}F transient before Fourier transform. A baseline correction was performed by fitting a first order polynomial to a region outside the peak of interest. The integrated and maximum ^{19}F signals were plotted over time to construct the NOE curves for the single-and dual-channel measurements, respectively. The acquired signal intensities were normalized with the intensity of the first non-hyperpolarized scan and used to fit the apparent σ following the equations published by J. Kim *et al*.[42] T_1 relaxation rates and concentrations of the ^{1}H and ^{19}F spins as well as water signal enhancement factors were used in the fitting. Control experiments were performed for all three sets of experiments under the conditions identical to each

of them, except that DNP samples were free of the TEMPOL radicals to eliminate hyperpolarization of water.

3.3. Results and Discussion

Transfer of water polarization to ligand ^{19}F spins was measured with the single-channel spectrometer to generate transient ^{19}F NOE buildup curves for TFBC binding. The acquired ^{19}F signal intensities were normalized with the signal intensity from the first non-hyperpolarized scan. The normalized ^{19}F signals measured after mixing with the hyperpolarized water for a preloaded sample of 15 mM TFBC in the absence and presence of 900 µM trypsin are represented by Figure 3.1 (a) and (b), respectively, both indicating a reduction in the ^{19}F signal intensity before approaching the thermal equilibrium. This reduction is a result of enhanced transferred magnetization from hyperpolarized water with a signal enhancement of ~1000x provided by D-DNP. A comparison between the D-DNP enhanced water signal and non-hyperpolarized water signal can be found in Figure A.3. As expected, the ^{19}F signal intensities for free TFBC were reduced by a larger magnitude compared to the those from measurements with trypsin due to binding. The lower S/N ratio in Figure 3.1 (b) and (d) is anticipated, as the ligand signals became broader and reduced in intensity upon binding.

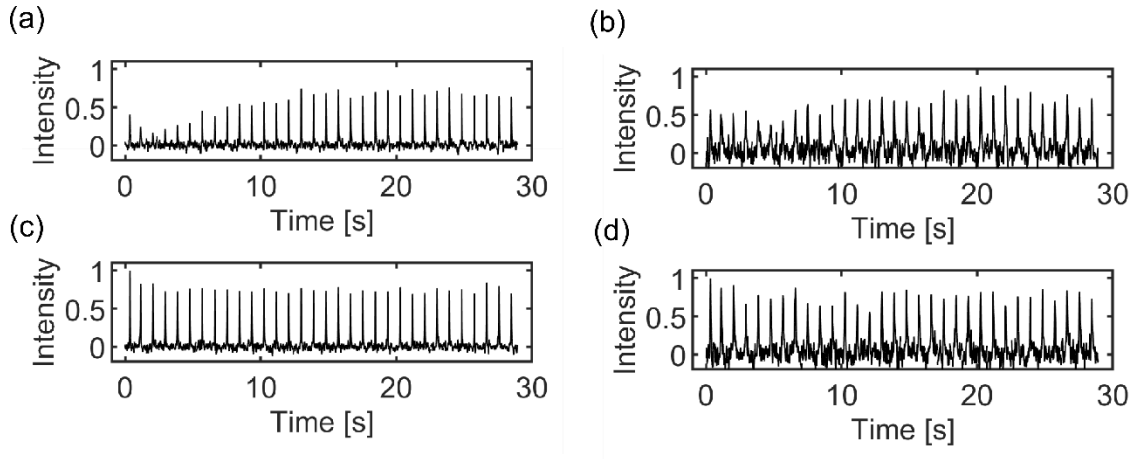

Figure 3.1 Stack plots of normalized **[19]**F signal intensity as a function of time measured with the single-channel spectrometer for a preloaded sample of 15 mM TFBC in the (a), (c) absence and (b), (d) presence of 900 μM trypsin. Spectra (a) and (b) were acquired after samples were mixed with hyperpolarized water, whereas (c) and (d) were measured after the decay of hyperpolarization.

The normalized ^{19}F signal intensities acquired were integrated and used to construct transient ^{19}F NOE buildup curves of TFBC in the absence and presence of trypsin as shown in Figure 3.2 (a) and (b), respectively. A stark contrast in the NOE buildup upon binding was observed when hyperpolarized water was introduced. The NOE buildup of free TFBC appeared negative due to a short τ_c for small molecules. A less negative buildup was observed with the addition of trypsin, which indicates the occurrence of binding corresponding to a slower molecular tumbling. The apparent σ was fitted from each of the NOE buildup curves following the equations published by J. Kim *et al*.[42] The apparent σ determined from the NOE buildup curves of free TFBC corresponds to the cross-relaxation rates of free ligands (σ_f). The apparent σ fitted from the NOE buildup curves in the presence of trypsin contains contributions from both free and bound ligands that can be represented by the fraction of free (χ_f) and bound (χ_b) ligands, respectively. The cross-relaxation rate for bound ligands (σ_b) was thus determined based on equation $\sigma = \chi_f\sigma_f + \chi_b\sigma_b$,[40] where χ_f and χ_b were calculated using previously published equations.[67] The NOE

buildup curves and the fitted cross-relaxation rates for individual single-channel experiments are shown with the experimental parameters in Appendix A.3.2. The average apparent σ fitted from NOE buildup curves represented by Figure 3.2 (a) and (b) was $4.69 \pm 0.30 \times 10^{-4}$ and $2.13 \pm 0.8 \times 10^{-4}$ s^{-1} M^{-1}, respectively, resulting in $\sigma_f = 4.69 \pm 0.30 \times 10^{-4}$ and $\sigma_b = -4.49 \pm 1.7 \times 10^{-3}$ s^{-1} M^{-1}. The positive and negative signs observed for σ_f and σ_b are in accordance with predictions made based on the relaxation theory. The cross-relaxation rate, an off-diagonal term in the relaxation matrix, is positive for small molecules with short τ_c ($\omega\tau_c < 1$, where ω is the Larmor frequency) and negative for macromolecules with long τ_c ($\omega\tau_c > 1$). Small molecules such as ligands, when bound to proteins, inherit the rotational correlation property of macromolecules, and acquire an opposite sign for the cross-relaxation rate. The confirmation of binding was manifested by this change in σ from positive to negative. The change in σ, 4.69×10^{-3} s^{-1} M^{-1}, is a significant difference of 2.9x compared to the standard deviation (SD) of the σ_b values.

D-DNP measurements performed with the single-channel spectrometer for a preloaded sample of 60 mM TFBC in the absence versus presence of 1.8 mM trypsin are presented in Figure 3.2 (c) and (d), suggesting a similar observation as illustrated in Figure 3.2 (a) and (b). The buildup of negative signals became lower in magnitude upon the addition of trypsin in the presence of hyperpolarized water. However, this change in the buildup is less prominent compared to that in Figure 3.2 (b) since a smaller fraction of bound ligands was present at the higher ligand concentration. The apparent σ from the NOE buildup curves represented by Figure 3.2 (c) and (d) was $4.64 \pm 0.29 \times 10^{-4}$ and $3.20 \pm 0.3 \times 10^{-4}$ s^{-1} M^{-1}, respectively, yielding $\sigma_f = 4.64 \pm 0.29 \times 10^{-4}$ s^{-1} and $\sigma_b = -4.62 \pm 1.1 \times 10^{-3}$ s^{-1} M^{-1} that are consistent with the values fitted from the curves

represented by Figure (a) and (b). The change in σ, 5.08 × 10^{-3} s^{-1} M^{-1}, again, is a significant difference of 4.5x compared to the SD of the σ_b values.

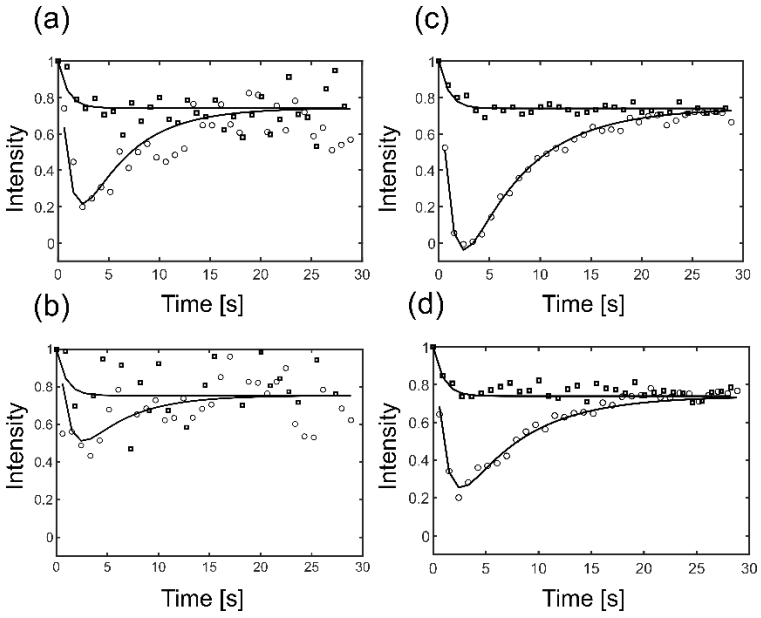

Figure 3.2 NOE buildup curves of integrated ^{19}F signals measured with the single-channel spectrometer for a preloaded sample of 15 mM TFBC in the (a) absence and (b) presence of 900 µM trypsin, or 60 mM TFBC in the (c) absence and (d) presence of 1.8 mM trypsin. Data points acquired after samples were mixed with hyperpolarized water and after decay of polarization are shown as circles and squares, respectively. The curves (ε = 843) in (a) and (b) used experiments with fitted σ = 4.72 × 10^{-4} and 2.25 × 10^{-4} s^{-1} M^{-1}, whereas those (ε = 1035) in (c) and (c) were from experiments with fitted σ = 4.65 × 10^{-4} and 2.76 × 10^{-4} s^{-1} M^{-1}, respectively.

When performing experiments with the single-channel spectrometer, water signal enhancement could not be simultaneously acquired with the ^{19}F signals in real time and need to be characterized in separate experiments. In this case, variations in the water signal enhancement factor used for fitting the cross-relaxation rates cannot be accounted for. This led to development of a dual-channel spectrometer in house to provide real-time characterization of water signal enhancement factors. The ^{19}F NOE buildup curves measured with the dual-channel spectrometer for a preloaded sample of 60 mM TFBC in the absence versus presence of 1.8 mM trypsin are

shown in Figure 3.3. This change in buildup is similar in magnitude to that in Figure 3.2 (d) under the same sample conditions. Due to the signal non-linearity observed at higher ^{1}H signal intensities, a correction factor was applied based on the calibration curve shown in Figure A.2. Experiments with the dual spectrometer produced an average apparent σ of $4.35 \pm 0.76 \times 10^{-4}$ and $2.81 \pm 0.7 \times 10^{-4}$ s^{-1} M^{-1} for measurements in the absence and presence of trypsin, respectively, resulting in an average σ_f of $4.35 \pm 0.8 \times 10^{-4}$ and σ_b of $-5.00 \pm 2.4 \times 10^{-3}$ s^{-1} M^{-1}. These values mostly agree with the values fitted from Figure 3.2. The difference in the fitted σ could be caused by the fact that water signal enhancement factors were not from real-time measurements for the latter. A summary of the NOE buildup curves and the fitted cross-relaxation rates for individual dual-channel experiments are shown with the experimental parameters in Appendix A.3.3. The change in σ, 5.44×10^{-3} s^{-1} M^{-1}, is a significant difference of 2.3x compared to the SD of the σ_b values. This change is a 9.7% difference from the change calculated for measurements represented by Figure 3.2(a) and (b) and a 7.0% difference from that for measurements represented by Figure 3.2 (c) and (d). Control experiments were performed under identical conditions as the single- and dual-channel experiments, except for the absence of radicals in the DNP samples. All control experiments shown in Figure A.5 show no difference for the NOE buildup curve measured after the sample was mixed with injected water sample and after the decay of hyperpolarization. This observation suggests that detection of binding through changes in NOE buildup requires the enhanced transferred magnetization from hyperpolarized water created by D-DNP. The advantage of high specificity using ^{19}F detection was manifested by the large signal from the protein protons that overlapped with ligand signals in the conventional ^{1}H-^{1}H water-LOGSY spectra shown in Figure A.4.

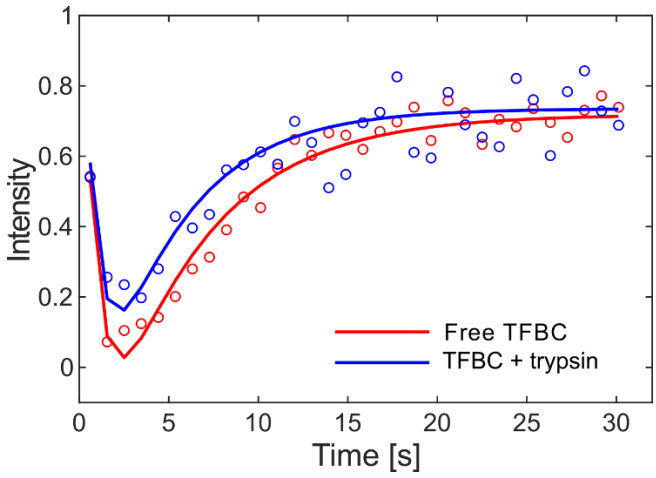

Figure 3.3 Comparison of ^{19}F NOE buildup curves as a function of time for a preloaded sample of 60 mM TFBC in the absence (red) and presence (blue) of 1.8 mM trypsin measured with the dual-channel spectrometer. Experimental trials with similar ε_{corr} of 1367 (red) and 1285 (blue) are compared.

The effect of different water signal enhancements on the ^{19}F NOE buildup was estimated by performing a simulation displayed in Figure 3.4. In the simulation, measurements from Figure 3.3 were fitted with ε = 1300 and ε = 1000 assuming the average σ of 4.35 ± 0.76 × 10^{-4} and 2.81 ± 0.7 × 10^{-4} s^{-1} M^{-1} for the NOE buildup curve in the absence and presence of trypsin, respectively, while all the other fitting parameters remained identical to the empirical ones from the measurements. For the NOE buildup of free TFBC, the simulated maximum buildup generated a relative intensity of 0 when ε = 1300 and 0.2 when ε = 1000. For the NOE buildup in the presence of 1.8 mM trypsin, the maximum buildup was predicted to have an approximate relative intensity of 0.2 when ε = 1300 and 0.4 when ε = 1000. This result is in alignment with the data observed at ε ~1000 as shown in Figure A.9. The simulation result suggests that a real-time measurement of water signal enhancement, which was accomplished by using a dual-channel spectrometer, can improve the accuracy of the fitted σ when there are variations in the water signal enhancement factors. These variations can be introduced when the percentage of water content or the radical

concentration differs. Small differences in water signal enhancement factors could result in a substantial change in the buildup curve that would affect the fitted rates.

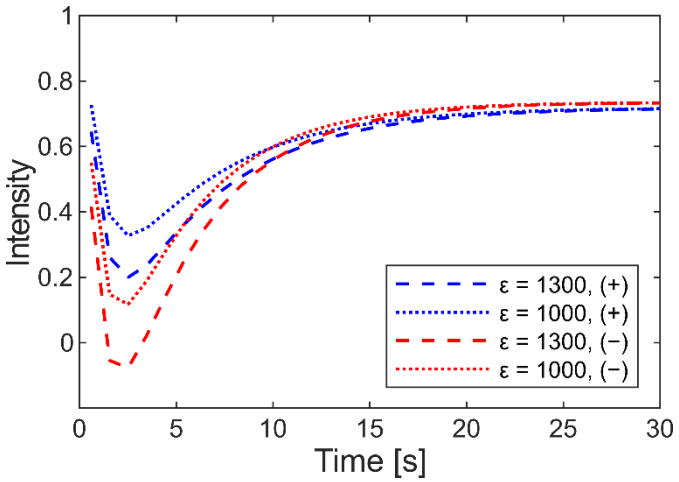

Figure 3.4 Simulation of the effect of water signal enhancement on ^{19}F NOE buildup for experiments with a preloaded sample of TFBC in the absence (red) and presence (blue) of trypsin. The dashed and dotted lines represent fits with ε =1300 and ε =1000, respectively. The simulated curves are fitted for the data sets represented in Figure 3.3 with concentration and relaxation parameters corresponding to each data set. The simulation assumes $\sigma = 4.35 \times 10^{-4}$ and 2.81×10^{-4} s^{-1} M^{-1} for fitting data from experiments with and without trypsin, respectively. These values are the average apparent σ measured with the dual-channel spectrometer.

Experiments with the dual-channel spectrometer were made possible by connecting the ^{1}H coil of the BBO probe to both channels through the use of a RF combiner and tuning it to the ^{19}F frequency. The off-tuned ^{1}H channel provided sufficient signal intensity for determining the water signal enhancement factors. The ligand concentration used in this study was optimized to be near the detection limit of each spectrometer. The dual-channel spectrometer was shown capable of detecting ligand ^{19}F signals as low as 6 mM, and the concentration detectable for the single-channel spectrometer is about four times lower in comparison. For measurements with the dual-channel spectrometer, the lowest attained ligand concentration excluded the possibility of producing a more prominent change by reducing ligand concentration or increasing protein concentration.

Experiments with an optimized concentration of 15 mM for the preloaded TFBC were performed with the single-channel spectrometer using a higher fraction of bound ligands to demonstrate a more prominent change. The final concentration of the protein counterpart in experiments with the dual-channel spectrometer was < 200 μM, which could theoretically be reduced by about 3 – 4 times for the single-channel spectrometer. On the other hand, water signal enhancement factors can only be measured separately when a single-channel is used. This could hamper the accuracy of fitted σ if there are variations in the water signal enhancement factors. The concentration requirement for both the protein and ligand when measuring with the dual-channel spectrometer could be lowered if the sensitivity of this spectrometer can be improved. The use of a more sensitive commercial dual-channel spectrometer or a probe with the ^{19}F-observe channel could improve the sensitivity by several fold. Nevertheless, the dual-channel spectrometer used in this study is more affordable and offers sufficient sensitivity for applications of this method. The required protein concentration could be further lowered by improving the water signal enhancement, which would enhance transfer of polarization and create a more prominent NOE buildup deviated from the thermal equilibrium for a specified protein concentration. This improvement could benefit proteins with poor solubility or those difficult to obtain.

The method developed here is suitable for detection of weak-to-medium binding as in typical water-LOGSY experiments. Its scope of applicability can be further expanded to detect binding of strong fluorinated ligands to protein targets when complemented with competitive binding, where the strong interaction can be indirectly probed through the NOE buildup change of a reporter ligand of weak or medium affinity.[71] The advantages of heteronuclear observation of ^{19}F nucleus have been demonstrated here, encompassing a reduced background and improved

specificity. The importance of developing a ^{19}F-based detection method is underscored by the popularity of fluorinated compounds in current HTS research.[83] The development of a method that utilizes hyperpolarized water to characterize binding has its unique advantages in comparison to direct hyperpolarization of ligands. Hyperpolarized water as a universal signal contrasting agent can be generated with high reproductivity and an extended lifetime of the ^{1}H spins by using D_2O or other methods.[71] Since only the lifetime of water protons is concerned when injecting hyperpolarized water, hyperpolarization of water with extended ^{1}H lifetimes has opened up new possibilities for detecting ligands of various types, including those with fast relaxation decay and low signal enhancement when directly hyperpolarized. Additionally, the equilibrium between the protein and ligand could be established prior to the hyperpolarized experiments, alleviating the restriction on the binding kinetics.

3.4. Conclusions

In summary, a ^{19}F NOE-based screening method for detection of binding through transfer of DNP-enhanced water polarization has been developed here. The binding is probed by quantifying the differential ^{1}H-^{19}F heteronuclear cross-relaxation rates of a fluorinated ligand in its free and bound states. The implementation of hyperpolarized water as a general signal enhancement agent has provided this method a broader scope of applicability to a wide range of ligands and binding kinetics. The necessity of measuring water signal enhancement in real time for accurate quantitation of cross relaxation rates was addressed by developing a dual-channel spectrometer capable of simultaneous ^{1}H and ^{19}F acquisition and illustrated with a simulation. The utility of this method for screening of protein-ligand interactions is highlighted by the ubiquity of fluorinated pharmaceuticals and the additional advantage of high specificity and sensitivity from

heteronuclear observation. This method can be complemented with competitive binding in the future to enable characterization of strongly binding fluorinated ligands using hyperpolarized water.

CHAPTER 4

SUMMARY AND CONCLUSIONS

Ligand-observed NMR is an effective HTS tool for studying protein-ligand interactions and screening of potential drug candidates, especially for evaluation of low-affinity interactions. The difference between the free and bound state of ligands is observed through perturbations on the NMR parameters, most of which are based on relaxation or NOE. A major limitation of ligand-observed NMR methods, however, is introduced by the low sensitivity of NMR. The incorporation of D-DNP can compensate this drawback by providing signal enhancement of several orders of magnitude compared to the conventional NMR.

Hyperpolarization provided by D-DNP can be coupled with competitive binding to develop a ^{1}H-based screening method that overcomes the difficulty of detecting high-affinity ligands experienced by most ligand-observed NMR methods. Binding of a strong ligand can be probed through perturbations on the transverse relaxation rate of a reporter ligand with single-scan CPMG experiments. The example for demonstration of this method was a ligand from the cGAS-STING pathway. This pathway is central to innate immune response and antitumor drug discovery. The development of a method that relies on ^{1}H detection is challenged by the larger signal interference from water protons that can overshadow the ligand signal of interest. The application of solvent suppression and selective excitation on the ligand resonance can effectively reduce the undesirable effect from water and produce resolvable ligand signals. On the other hand, ^{1}H-based detection has the benefits of broad applicability amenable to most ligands that contain protons. The ^{1}H relaxation-based method developed in this study has enabled detection of a diverse pool of ligands and evaluation of binding at various affinities.

While direct hyperpolarization of ligands with D-DNP is effective in most cases, characterization of ligands with fast longitudinal relaxation or binding in slow kinetics can be restricted. Hyperpolarization of water is a robust solution to these limitations, as it only relies on the relaxation of water protons and allows protein-ligand equilibrium to establish before injection. Transfer of DNP-enhanced water polarization to ligand spins can significantly enhance the NOE signals. Detection of the ^{19}F nucleus has the benefits of high specificity and sensitivity and is of great interest for drug discovery considering the prevalence of fluorinated pharmaceuticals. Hyperpolarized water created by D-DNP can be combined with ^{19}F NMR screening to develop a NOE-based method capable of detecting weak- to medium-affinity interactions through quantification of differential ^{1}H-^{19}F cross-relaxation rates upon binding. Characterization of real-time water signal enhancement, which is crucial to an accurate quantification, was accomplished with a dual-channel homemade spectrometer. This ^{19}F NOE-based screening also has the potential for detecting strong interactions by introducing competitive binding or for studying the binding of intracellular fluorinated ligands to protein targets.

In conclusion, ligand-observed methods have been developed to enable ^{1}H- and ^{19}F-based screening of ligands with the hyperpolarization provided by D-DNP. Each of these screening methods has the potential to expand the scope of applicability of hyperpolarized NMR in ligand-based screening. The use of D-DNP shortens the requirement of experimental time compared to conventional NMR, as the latter relies on signal averaging for sensitivity improvement. The signal enhancement created by D-DNP allows binding characterization at micromolar or sub-micromolar protein concentrations near physiological conditions, opening up the possibility for screening proteins that are difficult to purify or prone to aggregate.

REFERENCES

(1) Kim, K. M.; Yi, E. C.; Kim, Y. Mapping Protein Receptor–Ligand Interactions via in Vivo Chemical Crosslinking, Affinity Purification, and Differential Mass Spectrometry. *Methods* **2012**, *56* (2), 161–165.

(2) Fielding, L. NMR Methods for the Determination of Protein–Ligand Dissociation Constants. *Prog. Nucl. Magn. Reson. Spectrosc.* **2007**, *51* (4), 219–242.

(3) Du, X.; Li, Y.; Xia, Y.-L.; Ai, S.-M.; Liang, J.; Sang, P.; Ji, X.-L.; Liu, S.-Q. Insights into Protein–Ligand Interactions: Mechanisms, Models, and Methods. *Int. J. Mol. Sci.* **2016**, *17* (2), 144.

(4) Bourgeois, D.; Royant, A. Advances in Kinetic Protein Crystallography. *Curr. Opin. Struct. Biol.* **2005**, *15* (5), 538–547.

(5) Mittermaier, A.; Kay, L. E. New Tools Provide New Insights in NMR Studies of Protein Dynamics. *Science* **2006**, *312* (5771), 224–228.

(6) Henzler-Wildman, K.; Kern, D. Dynamic Personalities of Proteins. *Nature* **2007**, *450* (7172), 964–972.

(7) Sousa, S. F.; Cerqueira, N. M. F. S. A.; Fernandes, P. A.; Ramos, M. J. Virtual Screening in Drug Design and Development. *Comb. Chem. High Throughput Screen.* **2010**, *13* (5), 442–453.

(8) Sousa, S. F.; Ribeiro, A. J. M.; Coimbra, J. T. S.; Neves, R. P. P.; Martins, S. A.; Moorthy, N. S. H. N.; Fernandes, P. A.; Ramos, M. J. Protein-Ligand Docking in the New Millennium--a Retrospective of 10 Years in the Field. *Curr. Med. Chem.* **2013**, *20* (18), 2296–2314.

(9) Manly, C. J.; Chandrasekhar, J.; Ochterski, J. W.; Hammer, J. D.; Warfield, B. B. Strategies and Tactics for Optimizing the Hit-to-Lead Process and beyond--a Computational Chemistry Perspective. *Drug Discov. Today* **2008**, *13* (3–4), 99–109.

(10) Steinbrecher, T.; Labahn, A. Towards Accurate Free Energy Calculations in Ligand Protein-Binding Studies. *Curr. Med. Chem.* **2010**, *17* (8), 767–785.

(11) Goldflam, M.; Tarragó, T.; Gairí, M.; Giralt, E. NMR Studies of Protein–Ligand Interactions. In *Protein NMR Techniques*; Shekhtman, A., Burz, D. S., Eds.; Methods in Molecular Biology; Humana Press: Totowa, NJ, 2012; pp 233–259. 480-3_14.

(12) Wiseman, T.; Williston, S.; Brandts, J. F.; Lin, L. N. Rapid Measurement of Binding Constants and Heats of Binding Using a New Titration Calorimeter. *Anal. Biochem.* **1989**, *179* (1), 131–137.

(13) Chaires, J. B. Calorimetry and Thermodynamics in Drug Design. *Annu. Rev. Biophys.* **2008**, *37*, 135–151.

(14) Englebienne, P.; Hoonacker, A. V.; Verhas, M. Surface Plasmon Resonance: Principles, Methods and Applications in Biomedical Sciences. *Spectroscopy* **2003**, *17* (2–3), 255–273.

(15) Patching, S. G. Surface Plasmon Resonance Spectroscopy for Characterisation of Membrane Protein–Ligand Interactions and Its Potential for Drug Discovery. *Biochim. Biophys. Acta BBA - Biomembr.* **2014**, *1838* (1, Part A), 43–55.

(16) Ishii, K.; Noda, M.; Uchiyama, S. Mass Spectrometric Analysis of Protein–Ligand Interactions. *Biophys. Physicobiology* **2016**, *13*, 87–95.

(17) Nguyen, G. T. H.; Tran, T. N.; Podgorski, M. N.; Bell, S. G.; Supuran, C. T.; Donald, W. A. Nanoscale Ion Emitters in Native Mass Spectrometry for Measuring Ligand–Protein Binding Affinities. *ACS Cent. Sci.* **2019**, *5* (2), 308–318.

(18) Zhang, J.; Chalmers, M. J.; Stayrook, K. R.; Burris, L. L.; Garcia-Ordonez, R. D.; Pascal, B. D.; Burris, T. P.; Dodge, J. A.; Griffin, P. R. Hydrogen/Deuterium Exchange Reveals Distinct

Agonist/Partial Agonist Receptor Dynamics within the Intact Vitamin D Receptor/Retinoid X Receptor Heterodimer. *Struct. Lond. Engl. 1993* **2010**, *18* (10), 1332–1341.

(19) Dyachenko, A.; Goldflam, M.; Vilaseca, M.; Giralt, E. Molecular Recognition at Protein Surface in Solution and Gas Phase: Five VEGF Peptidic Ligands Show Inverse Affinity When Studied by NMR and CID-MS. *Biopolymers* **2010**, *94* (6), 689–700.

(20) Jameson, D. M.; Croney, J. C. Fluorescence Polarization: Past, Present and Future. *Comb. Chem. High Throughput Screen.* **2003**, *6* (3), 167–173.

(21) Lea, W. A.; Simeonov, A. Fluorescence Polarization Assays in Small Molecule Screening. *Expert Opin. Drug Discov.* **2011**, *6* (1), 17–32.

(22) Lee, Y.; Zeng, H.; Mazur, A.; Wegstroth, M.; Carlomagno, T.; Reese, M.; Lee, D.; Becker, S.; Griesinger, C.; Hilty, C. Hyperpolarized Binding Pocket Nuclear Overhauser Effect for Determination of Competitive Ligand Binding. *Angew. Chem. Int. Ed.* **2012**, *51* (21), 5179–5182.

(23) Wennerström, H. Nuclear Magnetic Relaxation Induced by Chemical Exchange. *Mol. Phys.* **1972**, *24* (1), 69–80.

(24) Carver, J. P.; Richards, R. E. A General Two-Site Solution for the Chemical Exchange Produced Dependence of T2 upon the Carr-Purcell Pulse Separation. *J. Magn. Reson.* **1972**, *6*, 89–105.

(25) McConnell, H. M. Reaction Rates by Nuclear Magnetic Resonance. *J. Chem. Phys.* **1958**, *28* (3), 430–431.

(26) Williamson, M. P. Using Chemical Shift Perturbation to Characterise Ligand Binding. *Prog. Nucl. Magn. Reson. Spectrosc.* **2013**, *73*, 1–16.

(27) Kodama, Y.; Takeuchi, K.; Shimba, N.; Ishikawa, K.; Suzuki, E.; Shimada, I.; Takahashi, H. Rapid Identification of Ligand-Binding Sites by Using an Assignment-Free NMR Approach. *J. Med. Chem.* **2013**, *56* (22), 9342–9350.

(28) Stockman, B. J.; Dalvit, C. NMR Screening Techniques in Drug Discovery and Drug Design. *Prog. Nucl. Magn. Reson. Spectrosc.* **2002**, *41* (3–4), 187–231.

(29) Salzmann, M.; Pervushin, K.; Wider, G.; Senn, H.; Wüthrich, K. TROSY in Triple-Resonance Experiments: New Perspectives for Sequential NMR Assignment of Large Proteins. *Proc. Natl. Acad. Sci.* **1998**, *95* (23), 13585–13590.

(30) Dias, D. M.; Ciulli, A. NMR Approaches in Structure-Based Lead Discovery: Recent Developments and New Frontiers for Targeting Multi-Protein Complexes. *Prog. Biophys. Mol. Biol.* **2014**, *116* (2), 101–112.

(31) Dalvit, C.; Flocco, M.; Knapp, S.; Mostardini, M.; Perego, R.; Stockman, B. J.; Veronesi, M.; Varasi, M. High-Throughput NMR-Based Screening with Competition Binding Experiments. *J. Am. Chem. Soc.* **2002**, *124* (26), 7702–7709.

(32) Tengel, T.; Fex, T.; Emtenäs, H.; Almqvist, F.; Sethson, I.; Kihlberg, J. Use of 19F NMR Spectroscopy to Screen Chemical Libraries for Ligands That Bind to Proteins. *Org. Biomol. Chem.* **2004**, *2* (5), 725–731.

(33) Levitt, Malcolm H. *Spin Dynamics: Basics of Nuclear Magnetic Resonance, 2nd Edition*; Wiley, 2008.

(34) Solomon, I. Relaxation Processes in a System of Two Spins. *Phys. Rev.* **1955**, *99* (2), 559–565.

(35) Lavalette, D.; Tétreau, C.; Tourbez, M.; Blouquit, Y. Microscopic Viscosity and Rotational Diffusion of Proteins in a Macromolecular Environment. *Biophys. J.* **1999**, *76* (5), 2744–2751.

(36) Gupta, A.; Stait-Gardner, T.; Moghaddam, M. J.; Price, W. S. Dipolar Relaxation Revisited: A Complete Derivation for the Two Spin Case. *Concepts Magn. Reson. Part A* **2015**, *44* (2), 74–113.

(37) Meiboom, S.; Gill, D. Modified Spin-Echo Method for Measuring Nuclear Relaxation Times. *Rev. Sci. Instrum.* **1958**, *29*, 688–691.

(38) Zhang, J.; Adrián, F. J.; Jahnke, W.; Cowan-Jacob, S. W.; Li, A. G.; Iacob, R. E.; Sim, T.; Powers, J.; Dierks, C.; Sun, F.; Guo, G.-R.; Ding, Q.; Okram, B.; Choi, Y.; Wojciechowski, A.; Deng, X.; Liu, G.; Fendrich, G.; Strauss, A.; Vajpai, N.; Grzesiek, S.; Tuntland, T.; Liu, Y.; Bursulaya, B.; Azam, M.; Manley, P. W.; Engen, J. R.; Daley, G. Q.; Warmuth, M.; Gray, N. S. Targeting Bcr-Abl by Combining Allosteric with ATP-Binding-Site Inhibitors. *Nature* **2010**, *463* (7280), 501–506.

(39) Congreve, M.; Rich, R. L.; Myszka, D. G.; Figaroa, F.; Siegal, G.; Marshall, F. H. Fragment Screening of Stabilized G-Protein-Coupled Receptors Using Biophysical Methods. *Methods Enzymol.* **2011**, *493*, 115–136.

(40) Wang, Y.; Hilty, C. Amplification of Nuclear Overhauser Effect Signals by Hyperpolarization for Screening of Ligand Binding to Immobilized Target Proteins. *Anal Chem* **2020**, 6.

(41) Nordstierna, L.; Yushmanov, P. V.; Furó, I. Solute-Solvent Contact by Intermolecular Cross-Relaxation. 2. The Water-Micelle Interface and the Micellar Interior. *J. Phys. Chem. B* **2006**, *110* (51), 25775–25781.

(42) Kim, J.; Liu, M.; Chen, H.-Y.; Hilty, C. Determination of Intermolecular Interactions Using Polarization Compensated Heteronuclear Overhauser Effect of Hyperpolarized Spins. *Anal. Chem.* **2015**, *87* (21), 10982–10987.

(43) Post, C. B. Exchange-Transferred NOE Spectroscopy and Bound Ligand Structure Determination. *Curr. Opin. Struct. Biol.* **2003**, *13* (5), 581–588.

(44) Ni, F.; Scheraga, H. A. Use of the Transferred Nuclear Overhauser Effect to Determine the Conformations of Ligands Bound to Proteins. *Acc. Chem. Res.* **1994**, *27* (9), 257–264.

(45) Sánchez-Pedregal, V. M.; Reese, M.; Meiler, J.; Blommers, M. J. J.; Griesinger, C.; Carlomagno, T. The INPHARMA Method: Protein-Mediated Interligand NOEs for Pharmacophore Mapping. *Angew. Chem. Int. Ed Engl.* **2005**, *44* (27), 4172–4175.

(46) Vaid, T. M.; Chalmers, D. K.; Scott, D. J.; Gooley, P. R. INPHARMA-Based Determination of Ligand Binding Modes at A1-Adrenergic Receptors Explains the Molecular Basis of Subtype Selectivity. *Chem. – Eur. J.* **2020**, *26* (51), 11796–11805.

(47) Mayer, M.; Meyer, B. Characterization of Ligand Binding by Saturation Transfer Difference NMR Spectroscopy. *Angew. Chem. Int. Ed.* **1999**, *38* (12), 1784–1788.

(48) Potenza, D.; Vasile, F.; Belvisi, L.; Civera, M.; Araldi, E. M. V. STD and TrNOESY NMR Study of Receptor-Ligand Interactions in Living Cancer Cells. *Chembiochem Eur. J. Chem. Biol.* **2011**, *12* (5), 695–699.

(49) Dalvit, C.; Fogliatto, G.; Stewart, A.; Veronesi, M.; Stockman, B. WaterLOGSY as a Method for Primary NMR Screening: Practical Aspects and Range of Applicability. *J. Biomol. NMR* **2001**, *21* (4), 349–359.

(50) Becker, W.; Bhattiprolu, K. C.; Gubensäk, N.; Zangger, K. Investigating Protein–Ligand Interactions by Solution Nuclear Magnetic Resonance Spectroscopy. *Chemphyschem* **2018**, *19* (8), 895–906.

(51) Coyne, K. New World-Record Magnet Fulfills Superconducting Promise. *National high magnetic field laboratory* **2017**.

(52) Hassan, A.; Quinn, C. M.; Struppe, J.; Sergeyev, I. V.; Zhang, C.; Guo, C.; Runge, B.; Theint, T.; Dao, H. H.; Jaroniec, C. P.; Berbon, M.; Lends, A.; Habenstein, B.; Loquet, A.; Kuemmerle, R.; Perrone, B.; Gronenborn, A. M.; Polenova, T. Sensitivity Boosts by the CPMAS CryoProbe for Challenging Biological Assemblies. *J. Magn. Reson. San Diego Calif 1997* **2020**, *311*, 106680.

(53) Bornet, A.; Melzi, R.; Perez Linde, A. J.; Hautle, P.; van den Brandt, B.; Jannin, S.; Bodenhausen, G. Boosting Dissolution Dynamic Nuclear Polarization by Cross Polarization. *J. Phys. Chem. Lett.* **2013**, *4* (1), 111–114.

(54) Warren, W. S.; Jenista, E.; Branca, R. T.; Chen, X. Increasing Hyperpolarized Spin Lifetimes Through True Singlet Eigenstates. *Science* **2009**, *323* (5922), 1711–1714.

(55) Can, T. V.; Ni, Q. Z.; Griffin, R. G. Mechanisms of Dynamic Nuclear Polarization in Insulating Solids. *J. Magn. Reson. San Diego Calif 1997* **2015**, *253*, 23–35.

(56) Abragam, A.; Goldman, M. Principles of Dynamic Nuclear Polarisation. *Rep. Prog. Phys.* **1978**, *41* (3), 395–467.

(57) Wenckebach, W. Th. Dynamic Nuclear Polarization via Thermal Mixing: Beyond the High Temperature Approximation. *J. Magn. Reson.* **2017**, *277*, 68–78.

(58) Hofer, P.; Carl, P.; Guthausen, G.; Prisner, T.; Reese, M.; Carlomagno, T.; Griesinger, C.; Bennati, M. Studies of dynamic nuclear polarization with nitroxides in aqueous solutio

(59) Chen, H.-Y.; Hilty, C. Implementation and Characterization of Flow Injection in Dissolution Dynamic Nuclear Polarization NMR Spectroscopy. *ChemPhysChem* **2015**, *16* (12), 2646–2652.

(60) Kim, Y.; Liu, M.; Hilty, C. Parallelized Ligand Screening Using Dissolution Dynamic Nuclear Polarization. *Anal. Chem.* **2016**, *88* (22), 11178–11183.

(61) Pellecchia, M.; Bertini, I.; Cowburn, D.; Dalvit, C.; Giralt, E.; Jahnke, W.; James, T. L.; Homans, S. W.; Kessler, H.; Luchinat, C.; Meyer, B.; Oschkinat, H.; Peng, J.; Schwalbe, H.; Siegal, G. Perspectives on NMR in Drug Discovery: A Technique Comes of Age. *Nat. Rev. Drug Discov.* **2008**, *7* (9), 738–745.

(62) Entzeroth, M.; Flotow, H.; Condron, P. Overview of High-Throughput Screening. *Curr. Protoc. Pharmacol.* **2009**, *Chapter 9*, Unit 9.4.

(63) Lepre, C. A.; Moore, J. M.; Peng, J. W. Theory and Applications of NMR-Based Screening in Pharmaceutical Research. *Chem. Rev.* **2004**, *104* (8), 3641–3676.

(64) Dalvit, C. Theoretical Analysis of the Competition Ligand-Based NMR Experiments and Selected Applications to Fragment Screening and Binding Constant Measurements. *Concepts Magn. Reson. Part A* **2008**, *32A* (5), 341–372.

(65) Huang, R.; Bonnichon, A.; Claridge, T. D. W.; Leung, I. K. H. Protein-Ligand Binding Affinity Determination by the WaterLOGSY Method: An Optimised Approach Considering Ligand Rebinding. *Sci. Rep.* **2017**, *7* (1), 43727.

(66) Dalvit, C.; Flocco, M.; Veronesi, M.; Stockman, B. J. Fluorine-NMR Competition Binding Experiments for High-Throughput Screening of Large Compound Mixtures. *Comb. Chem. High Throughput Screen.* **2002**, *5* (8), 605–611.

(67) Kim, Y.; Hilty, C. Affinity Screening Using Competitive Binding with Fluorine-19 Hyperpolarized Ligands. *Angew. Chem. Int. Ed.* **2015**, *54* (16), 4941–4944.

(68) Wang, Y.-S.; Liu, D.; Wyss, D. F. Competition STD NMR for the Detection of High-Affinity Ligands and NMR-Based Screening. *Magn. Reson. Chem. MRC* **2004**, *42* (6), 485–489.

(69) Dalvit, C.; Fasolini, M.; Flocco, M.; Knapp, S.; Pevarello, P.; Veronesi, M. NMR-Based Screening with Competition Water-Ligand Observed via Gradient Spectroscopy Experiments: Detection of High-Affinity Ligands. *J. Med. Chem.* **2002**, *45* (12), 2610–2614.

(70) Buratto, R.; Bornet, A.; Milani, J.; Mammoli, D.; Vuichoud, B.; Salvi, N.; Singh, M.; Laguerre, A.; Passemard, S.; Gerber-Lemaire, S.; Jannin, S.; Bodenhausen, G. Drug Screening Boosted by Hyperpolarized Long-Lived States in NMR. *Chemmedchem* **2014**, *9* (11), 2509–2515.

(71) Chappuis, Q.; Milani, J.; Vuichoud, B.; Bornet, A.; Gossert, A. D.; Bodenhausen, G.; Jannin, S. Hyperpolarized Water to Study Protein–Ligand Interactions. *J. Phys. Chem. Lett.* **2015**, *6* (9), 1674–1678.

(72) Li, T.; Cheng, H.; Yuan, H.; Xu, Q.; Shu, C.; Zhang, Y.; Xu, P.; Tan, J.; Rui, Y.; Li, P.; Tan, X. Antitumor Activity of CGAMP via Stimulation of CGAS-CGAMP-STING-IRF3 Mediated Innate Immune Response. *Sci. Rep.* **2016**, *6*, 19049.

(73) Liu, X.; Wang, C. The Emerging Roles of the STING Adaptor Protein in Immunity and Diseases. *Immunology* **2016**, *147* (3), 285–291.

(74) Li, X.; Shu, C.; Yi, G.; Chaton, C. T.; Shelton, C. L.; Diao, J.; Zuo, X.; Kao, C. C.; Herr, A. B.; Li, P. Cyclic GMP-AMP Synthase Is Activated by Double-Stranded DNA-Induced Oligomerization. *Immunity* **2013**, *39* (6), 1019–1031.

(75) Shang, G.; Zhang, C.; Chen, Z. J.; Bai, X.; Zhang, X. Cryo-EM Structures of STING Reveal Its Mechanism of Activation by Cyclic GMP–AMP. *Nature* **2019**, *567* (7748), 389–393.

(76) Zhang, X.; Shi, H.; Wu, J.; Zhang, X.; Sun, L.; Chen, C.; Chen, Z. J. Cyclic GMP-AMP Containing Mixed Phosphodiester Linkages Is An Endogenous High-Affinity Ligand for STING. *Mol. Cell* **2013**, *51* (2), 226–235.

(77) Shu, C.; Yi, G.; Watts, T.; Kao, C. C.; Li, P. Structure of STING Bound to C-Di-GMP Reveals the Mechanism of Cyclic Dinucleotide Recognition by the Immune System. *Nat. Struct. Mol. Biol.* **2012**, *19* (7), 722–724.

(78) Mandal, R.; Pham, P.; Hilty, C. Characterization of Protein–Ligand Interactions by SABRE. *Chem. Sci.* **2021**, *12* (39), 12950–12958.

(79) Harris, T.; Szekely, O.; Frydman, L. On the Potential of Hyperpolarized Water in Biomolecular NMR Studies. *J. Phys. Chem. B* **2014**, *118* (12), 3281–3290.

(80) Olsen, G.; Markhasin, E.; Szekely, O.; Bretschneider, C.; Frydman, L. Optimizing Water Hyperpolarization and Dissolution for Sensitivity-Enhanced 2D Biomolecular NMR. *J. Magn. Reson.* **2016**, *264*, 49–58.

(81) Kim, J.; Liu, M.; Hilty, C. Modeling of Polarization Transfer Kinetics in Protein Hydration Using Hyperpolarized Water. *J. Phys. Chem. B* **2017**, *121* (27), 6492–6498.

(82) Szekely, O.; Olsen, G. L.; Novakovic, M.; Rosenzweig, R.; Frydman, L. Assessing Site-Specific Enhancements Imparted by Hyperpolarized Water in Folded and Unfolded Proteins by 2D HMQC NMR. *J. Am. Chem. Soc.* **2020**, *142* (20), 9267–9284.

(83) Lee, Y.; Zeng, H.; Ruedisser, S.; Gossert, A. D.; Hilty, C. Nuclear Magnetic Resonance of Hyperpolarized Fluorine for Characterization of Protein–Ligand Interactions. *J. Am. Chem. Soc.* **2012**, *134* (42), 17448–17451.

APPENDIX A

SUPPORTING INFORMATION FOR "^{19}F NOE-BASED SCREENING FOR QUANTIFYING BINDING WITH HYPERPOLARIZED WATER"

A.1 Instrumentation and Calibration

A.1.1. Construction of a Dual-channel Spectrometer

A ^{1}H-^{19}F spectrometer was built in house to achieve dual-channel acquisition for real-time characterization of water signal enhancement. Its configuration is shown in Figure A.1. A radio frequency (RF) synthesizer (Programmed Test Sources, Littleton, MA, Model D620) was used to generate a 356 MHz base frequency, which was mixed using mixers (Mini-Circuits, Brooklyn, NY, Model ZX05-1L-S^{+}) with additional frequencies emitted by the RP and PB board to produce 376.4 MHz and 400.1 MHz for the ^{19}F and ^{1}H channels, respectively. The desirable frequency of input signals was filtered with filters (K&L Microwave, Salisbury, MD) centered at the 376 MHz and 400 MHz before passing through amplifiers (TOMCO Technologies, Stepney, Australia, Model BT00250-Gamma and BT00100-Gamma). The amplified signals from both channels were combined through a RF combiner/splitter (Mini-Circuits, Model ZA2CS-62-40W^{+}) that was connected to the ^{1}H coil of the BBO probe tuned to the ^{19}F frequency. The returned signals from the sample were then split into two ways by the same RF combiner/splitter before each stream of signals entered a circuit box equipped with a quarter-wavelength cable and cross-diodes connected to the ground. The TX/RX switches (Mini-Circuits, Model ZX80-DR230-S^{+}) were turned on upon arrival of the signals, which were then selected by the filters (K&L Microwave) for desirable frequency ranges. The filtered signals were amplified by preamplifiers (Mini-Circuits, Model ZX60-P103LN^{+} and ZFL-500LN^{+}) and mixed with 356 MHz to demodulate and passed along the bandpass filters (Mini-Circuits, Model 15542, 19.2 –23.6 MHz). The demodulated ^{19}F signal was

measured using a RP board capable of generating pulses and receiving signals, while the ^{1}H channel utilized a pulse-generating PB board separate from the signal-receiving RP-RX board.

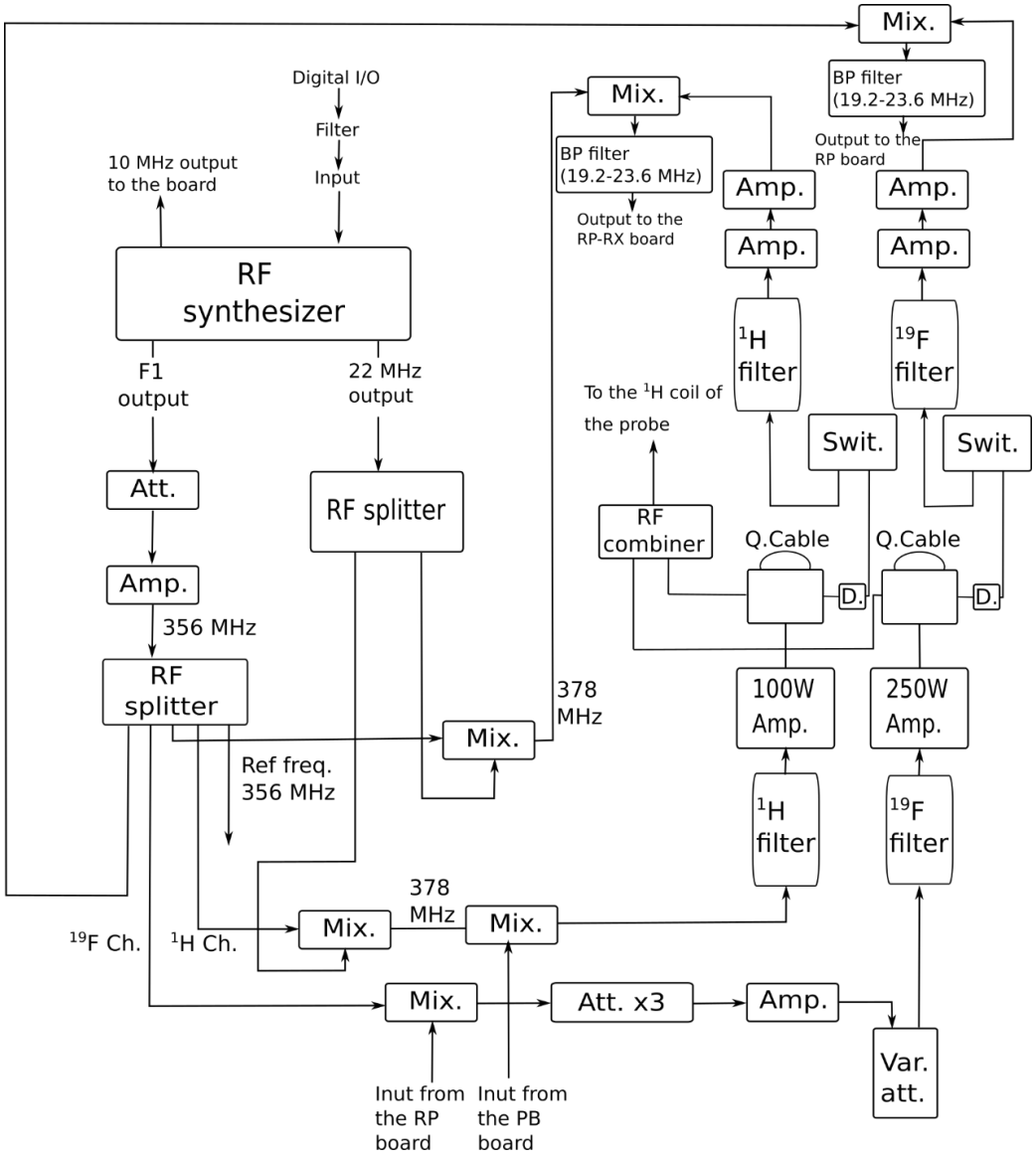

Figure A.1 Configuration of the dual-channel spectrometer. Additional abbreviations were used for attenuators (Att.), amplifiers (Amp.), mixers (Mix.), switches (Swit.), quarter-wavelength cables (Q. coil), cross-diodes (D.), and bandpass (BP) filters. All boards are controlled by digital I/O through LabVIEW.

A.1.2. Calibration for ^{1}H Signal Linearity

A potential non-linearity of ^{1}H signals at higher intensities can result in an underestimated water signal enhancement factor. A calibration curve, shown in Figure A.2., was measured to evaluate the signal linearity of the ^{1}H channel at different observed intensities I_0 and to account for any non-linearity produced. A H_2O sample was excited at different pulse lengths θ to cover a wide range of observed signal intensities I_0, which were converted to normalized intensities I using the equation $I = I_0/\sin(\theta)$. The average of the normalized intensities in the linear region of the calibration curve was calculated to be 4.18×10^{12}. The observed intensities of hyperpolarized and non-hyperpolarized water signals from each experiment were interpolarted to obtain the corresponding normalized intensities based on the curve. These normalized intensities were then compared against the average normalized intensity of the linear region (4.18×10^{12}) to determine the correction factor needed for the water signal enhancement from each experiment. This correction factor was applied to the raw water signal enhancement (ε_{raw}) for determining the corrected water signal enhancement (ε_{corr}).

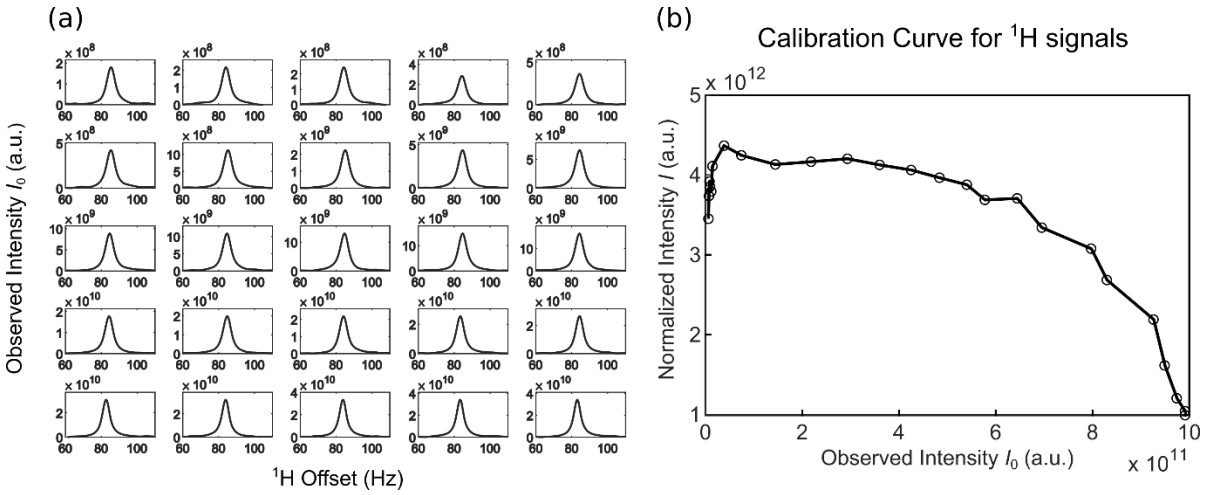

Figure A.2 ^{1}H signal linearity calibration. (a) Spectra of ^{1}H signal intensity of a pure H_2O sample acquired with the dual-channel spectrometer for signal linearity calibration. Varying excitation angles were applied to create an array of observed ^{1}H signal intensities I_0 encompassing the intensity range of both hyperpolarized and non-hyperpolarized water signals. (b) Calibration curve of signal linearity for the ^{1}H channel of the dual-channel spectrometer. Integrated signal intensity of individual scans in (a) was normalized by factoring in the corresponding sine value of the excitation angle to calculate the normalized intensities *I*. The fitted curve is an interpolation of the normalized intensities based on observed intensities.

A.2 Supplementary Experiments

A.2.1. Water Signal Enhancement Provided by D-DNP

Water signal enhancement provided by D-DNP was characterized by applying a 0.1° excitation pulse on the water resonance and comparing the hyperpolarized ^{1}H water spectrum to a thermally polarized water spectrum. The achievable enhancement was >1000x in most experiments. A comparison between signals of hyperpolarized water and non-hyperpolarized water is shown in Figure A.3.

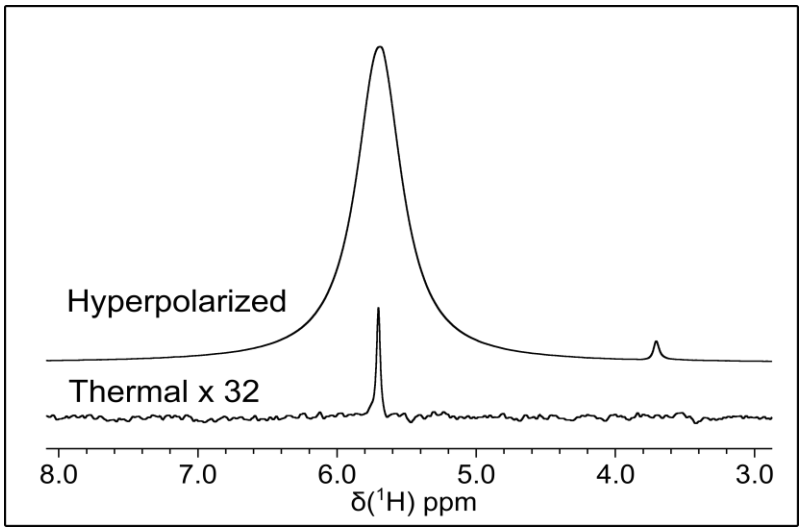

Figure A.3 Comparison between the hyperpolarized ^{1}H water spectrum and non-hyperpolarized water spectrum acquired using a 0.1° flip angle pulse. Hyperpolarization of water was created using a sample of 1:1 v/v mixture of H_2O:d6-DMSO containing 15 mM TEMPOL. The non-hyperpolarized spectrum here is displayed with a 32x scaling factor.

A.2.2 Conventional ^{1}H-^{1}H Water-LOGSY

A conventional ^{1}H-^{1}H water-LOGSY experiment was performed with 1 mM benzamidine in the absence and presence of 50 μM trypsin without hyperpolarization. The pulse sequence[1] used in conventional water-LOGSY measurements is displayed in Figure A.4 (a). The acquired spectrum, as shown in Figure A.4 (b), indicates an NOE sign change from negative to positive upon binding. This observation is anticipated, as ligands in a bound complex yields a longer τ_c and less negative NOE enhancement. The ligand signals from the ligand aromatic protons were interfered by the proton signals from the protein.

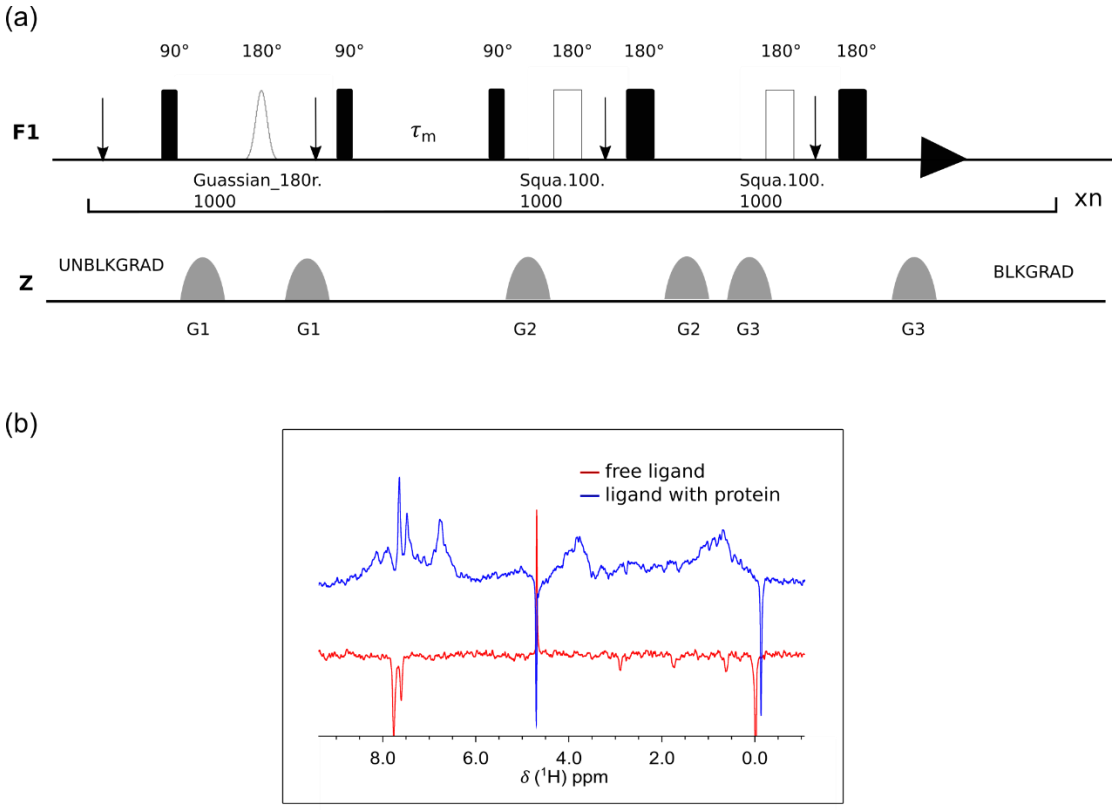

Figure A.4 Conventional water-LOGSY experiments (a) pulse sequence used for measurements (b) ^{1}H-^{1}H water-LOGSY spectrum of 1 mM benzamidine in the absence (red) versus presence (blue) of 50 μM trypsin. 1 mM sodium trimethylsilylpropanesulfonate (DSS) was used as a phase reference and is expected to adopt the same phase as free ligands.

A.2.3. Control experiments

Control experiments were performed for three sets of hyperpolarized experiments under the conditions identical to each of them, except that the TEMPOL radicals were eliminated from the DNP sample to ensure water protons remain non-hyperpolarized. Experimental parameters in control trials are listed in Table A.1 below. The acquired NOE curves are collectively shown in Figure A.5. No difference was observed between experiments in the absence and presence of trypsin when water was not hyperpolarized.

Table A.1 Summary of experimental parameters used in control experiments. The experimental conditions in all control trials are identical to those in the NOE experiments, except that the radicals are absent in the DNP samples. Control experiments 1-2, 3-4, and 5-6 are paralleled to experiments measured with the single-channel spectrometer at relatively high and low fraction of bound TFBC, and the experiments with the dual-channel spectrometer, respectively. Each pair contains one experiment with free TFBC and another in the presence of trypsin. The water signal enhancement factor $\varepsilon = 1$ was used to fit all the experimental trials in this table. For trials with free TFBC, r_F = 0.602 s^{-1} and r_H = 0.106 s^{-1} were applied in the fitting. For trials with bound TFBC, r_F = 0.554 s^{-1} and r_H = 0.096 s^{-1} were assumed instead. These relaxation parameters were determined from samples with similar conditions and then used for each trial here.

	[TFBC] (mM)	**[Trypsin] (mM)**	c_F **(mM)**	c_H **(M)**	χ_b	ζ
Control 1	15	0	4.04	1.65		11
Control 2	15	0.9	4.31	1.76	0.0517	10
Control 3	60	0	16.4	1.64		11
Control 4	60	1.8	17.4	2.11	0.0284	10
Control 5	60	0	16.2	1.79		11
Control 6	60	1.8	12.7	1.96	0.0282	14

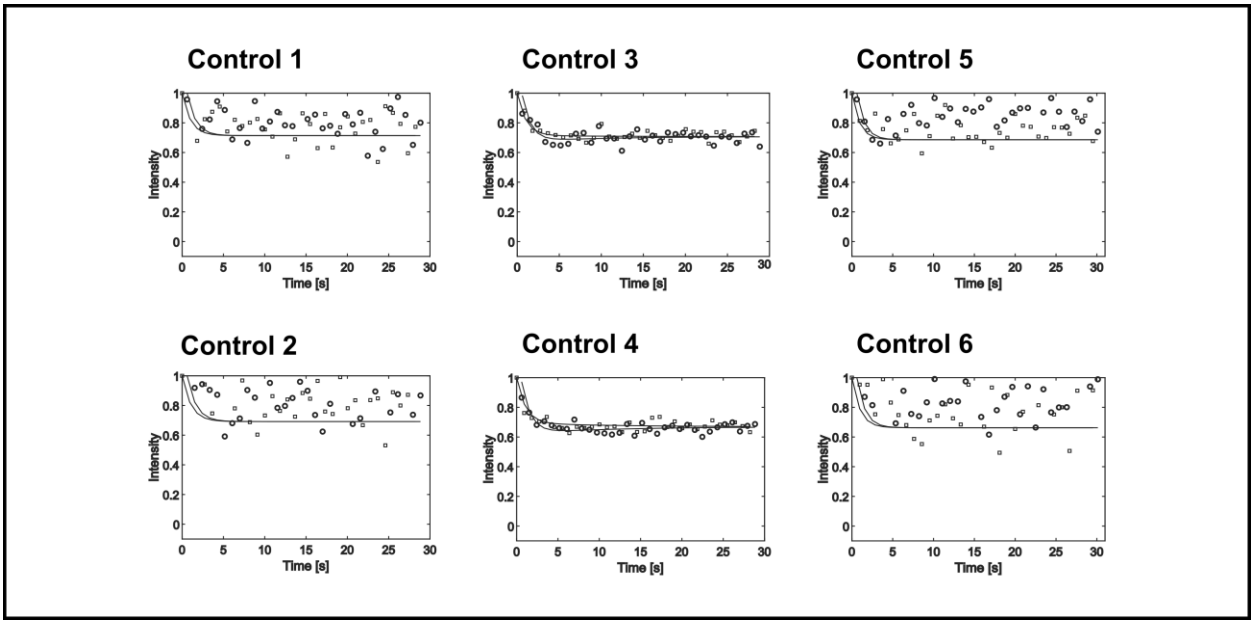

Figure A.5 NOE buildup curves of ^{19}F signals for all the control trials shown in Table A.1. The intensity values in Control 1-4 are from integrated ^{19}F signals normalized with the integration of the first non-hyperpolarized scan, whereas those in Control 5 and 6 are maximum ^{19}F intensities normalized with the maximum of the first non-hyperpolarized scan. Data points acquired after preloaded samples were mixed with DNP samples and at thermal equilibrium are shown as circles and squares, respectively. All control experiments are fitted with ε = 1 and the relaxation parameters described in Table A.1.

A.3 Supplementary Data

NOE buildup curves were monitored using both the single- and dual-channel spectrometer. A collection of buildup curves from each experimental trials is displayed in Figure A.6 – 8. The relaxation and concentration parameters of each spins as well as water signal enhancement factors used for fitting σ are included in Table A.2 – 4.

A.3.1 Measurements with the Single-channel Spectrometer

Measurements were performed with the single-channel spectrometer for a preloaded sample of 15 mM TFBC in the absence and presence of 900 μM trypsin. The average ε = 843 was

used to fit the σ for all the experimental trials shown in Table A.2. The average final concentration of TFBC after injection was 1.50 ± 0.18 mM among the following trials. The fitted NOE curves of TFBC in the absence and presence of trypsin are displayed in Figure A.6.

Table A.2 ^{1}H-^{19}F cross-relaxation rates of for a preloaded sample of 15 mM TFBC in the absence and presence of 900 μM trypsin acquired with the single-channel spectrometer. The experimental parameters used for fitting σ are included below (ε = 843 was used).

	r_F (s^{-1})	r_H (s^{-1})	c_F (mM)	c_H (M)	χ_b	σ ($s^{-1}\,M^{-1}$)	σ_f ($s^{-1}\,M^{-1}$)	σ_b ($s^{-1}\,M^{-1}$)	ζ
trial 1_F	0.690	0.199	4.23	1.66		4.94×10^{-4}	4.94×10^{-4}		11
trial 2_F	0.749	0.209	4.60	1.58		4.41×10^{-4}	4.41×10^{-4}		10
trial 3_F	0.671	0.207	4.98	1.58		4.71×10^{-4}	4.71×10^{-4}		9
trial 4_B	0.699	0.182	3.48	1.59	0.0506	9.80×10^{-5}		-6.86×10^{-3}	13
trial 5_B	0.704	0.218	4.40	1.67	0.0518	2.25×10^{-4}		-4.24×10^{-3}	10
trial 6_B	0.798	0.185	5.37	1.32	0.0526	3.03×10^{-4}		-2.69×10^{-3}	10
trial 7_B	0.698	0.238	4.42	2.13	0.0517	2.28×10^{-4}		-4.18×10^{-3}	10
Mean ± SD	0.716 ± 0.043	0.205 ± 0.019	4.50 ± 0.55	1.65 ± 0.24	0.0517 ± 8×10^{-4}		4.69 ± 0.30×10^{-4}	-4.49 ± 1.73×10^{-3}	10 ± 2

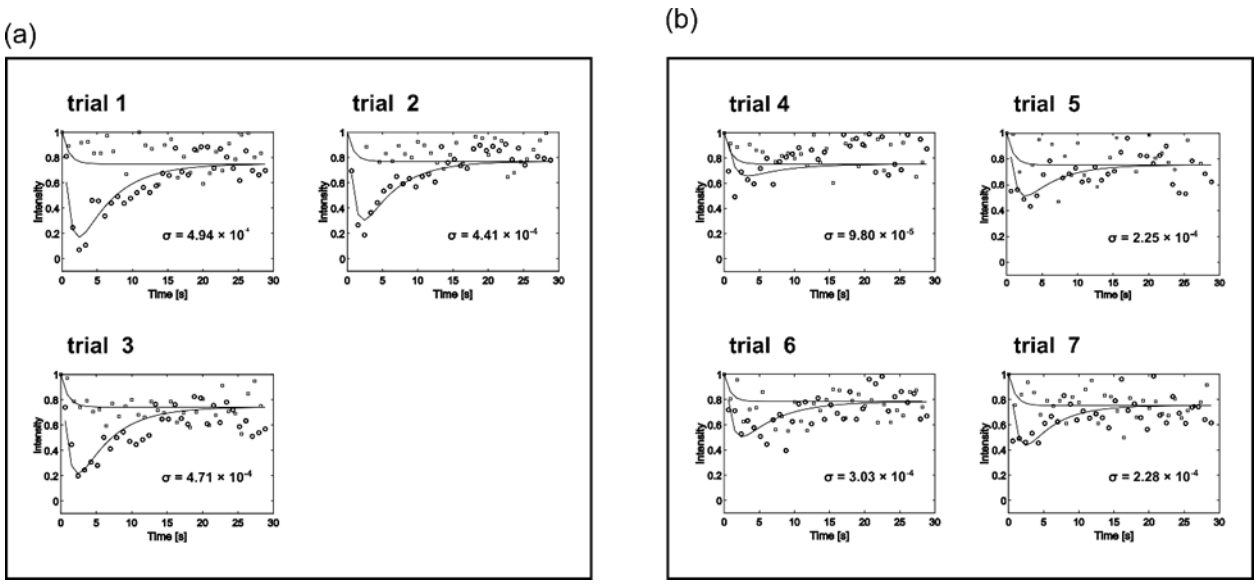

Figure A.6 NOE buildup curves of integrated ^{19}F signals for all the experimental trials shown in Table A.2. The intensity values are normalized with the integrated signal of the first non-hyperpolarized scan and fitted with the average ε = 843. The apparent σ was characterized with the single-channel spectrometer for a preloaded sample of 15 mM TFBC in the (a) absence and (b) presence of 900 μM trypsin and displayed accordingly for each trial. Data points acquired after samples were mixed with hyperpolarized water and after the decay of hyperpolarization are shown as circles and squares, respectively.

Another set of measurements were performed with the single-channel spectrometer for a preloaded sample of 60 mM TFBC in the absence and presence of 1.8 mM trypsin. The average ε = 1035 was used to fit the σ for all the experimental trials shown in Table A.3. The average final concentration of TFBC after injection was 1.50 ± 0.18 mM among the following trials. The fitted NOE curves of TFBC in the absence and presence of trypsin are displayed in Figure A.7.

Table A.3 ^{1}H-^{19}F cross-relaxation rates for a preloaded sample of 60 mM TFBC in the absence and presence of 1.8 mM trypsin acquired with the single-channel spectrometer. The experimental parameters used for fitting σ are included below (ε = 1035 was used).

	r_F (s^{-1})	r_H (s^{-1})	c_F (mM)	c_H (M)	χ_b	σ ($s^{-1} M^{-1}$)	σ_f ($s^{-1} M^{-1}$)	σ_b ($s^{-1} M^{-1}$)	ζ
trial 1_F	0.665	0.146	20.0	1.67		4.96×10^{-4}	4.96×10^{-4}		9
trial 2_F	0.632	0.155	20.0	1.80		4.27×10^{-4}	4.27×10^{-4}		9
trial 3_F	0.665	0.162	17.4	1.81		4.65×10^{-4}	4.65×10^{-4}		10
trial 4_F	0.631	0.155	22.4	1.55		4.68×10^{-4}	4.68×10^{-4}		8
trial 5_B	0.663	0.162	19.0	1.94	0.0285	2.76×10^{-4}		-6.12×10^{-3}	9
trial 6_B	0.637	0.138	17.4	1.64	0.0284	3.30×10^{-4}		-4.25×10^{-3}	10
trial 7_B	0.640	0.136	12.1	1.99	0.0281	3.56×10^{-4}		-3.39×10^{-3}	15
trial 8_B	0.609	0.135	16.8	1.99	0.0284	3.17×10^{-4}		-4.71×10^{-3}	11
Mean ± SD	0.643 ± 0.020	0.149 ± 0.011	18.1 ± 3.1	1.80 ± 0.17	0.0284 ± 2×10^{-4}		4.64 ± 0.29×10^{-4}	-4.62 ± 1.14×10^{-3}	10 ± 2

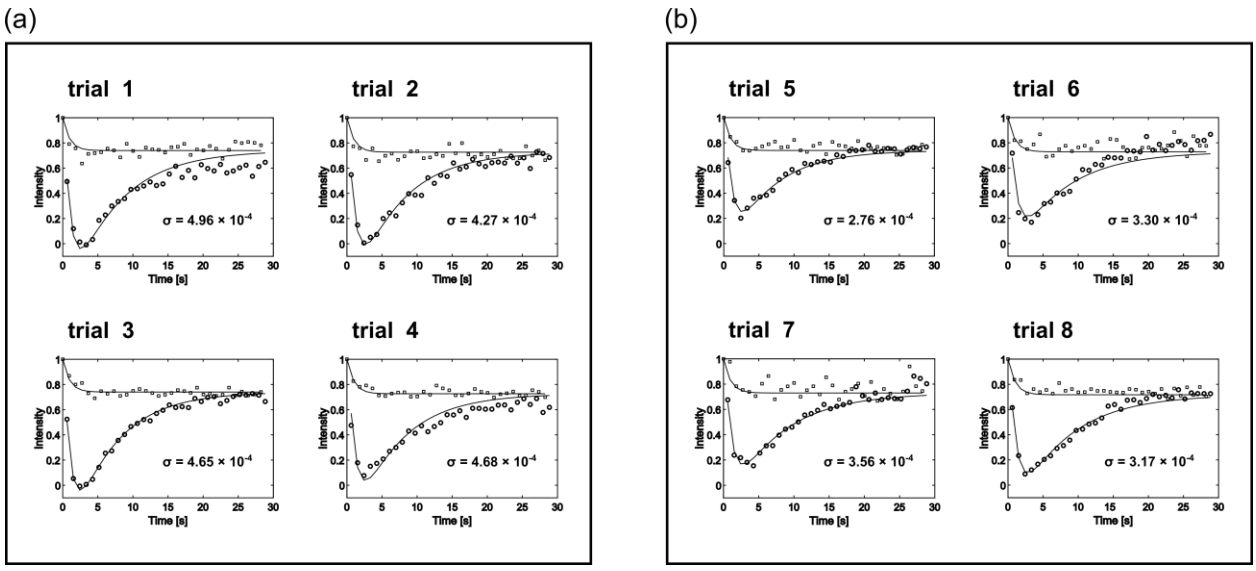

Figure A.7 NOE buildup curves of integrated ^{19}F signals for all the experimental trials shown in Table A.3. The intensity values are normalized with the integrated signal of the first non-hyperpolarized scan and fitted with the average ε of 1035. The apparent σ was characterized with the single-channel spectrometer for a preloaded sample of 60 mM TFBC in the (a) absence and (b) presence of 1.8 mM trypsin and displayed accordingly for each trial. Data points acquired after samples were mixed with hyperpolarized water and after the decay of hyperpolarization are shown as circles and squares, respectively.

A.3.2. Measurements with the Dual-channel Spectrometer

Experiments were measured with the dual-channel spectrometer for a preloaded sample of 60 mM TFBC in the absence and presence of 1.8 mM trypsin. Both ε before and after linearity correction were used to fit the σ for all the experimental trials shown in Table A.4. The average final concentration of TFBC after injection is 5.88 ± 0.88 mM among the following trials. The fitted NOE curves for TFBC in the absence and presence of trypsin are displayed in Figure A.8.

Table A.4 ^{1}H-^{19}F cross-relaxation rates for a preloaded sample of 60 mM TFBC in the absence and presence of 1.8 mM trypsin acquired with the dual-channel spectrometer. The experimental parameters used for fitting σ are included below. The σ before and after the correction of water signal enhancement factor were determined from the ε_{raw} and ε_{corr}, respectively.

	r_F (s^{-1})	r_H (s^{-1})	c_F (mM)	c_H (M)	χ_b	ε_{raw}	ε_{corr}	σ_{raw} ($s^{-1} M^{-1}$)	σ_{corr} ($s^{-1} M^{-1}$)	σ_f ($s^{-1} M^{-1}$)	σ_b ($s^{-1} M^{-1}$)	ζ
trial 1_F	0.642	0.162	17.9	1.44		803	947	6.26×10^{-4}	5.31×10^{-4}	5.31×10^{-4}		10
trial 2_F	0.709	0.235	18.3	1.56		760	897	5.32×10^{-4}	4.51×10^{-4}	4.51×10^{-4}		10
trial 3_F	0.690	0.213	17.6	1.83		820	1014	5.05×10^{-4}	4.08×10^{-4}	4.08×10^{-4}		10
trial 4_F	0.677	0.181	23.1	1.70		868	1367	5.52×10^{-4}	3.50×10^{-4}	3.50×10^{-4}		8
trial 5_B	0.677	0.202	13.9	2.00	0.0283	693	863	4.55×10^{-4}	3.77×10^{-4}		-1.61×10^{-3}	13
trial 6_B	0.748	0.222	14.4	1.74	0.0283	845	1025	2.93×10^{-4}	2.41×10^{-4}		-6.43×10^{-3}	13
trial 7_B	0.774	0.266	15.3	2.01	0.0283	619	739	2.23×10^{-4}	1.87×10^{-4}		-8.39×10^{-3}	12
trial 8_B	0.698	0.194	20.1	1.66	0.0285	940	1470	4.98×10^{-4}	3.18×10^{-4}		-3.66×10^{-3}	9
trial 9_B	0.715	0.217	16.5	1.86	0.0284	1002	1677	4.29×10^{-4}	2.56×10^{-4}		-5.87×10^{-3}	11
trial 10_B	0.719	0.221	19.3	1.86	0.0285	779	1285	5.04×10^{-4}	3.05×10^{-4}		-4.12×10^{-3}	9
Mean ± SD	0.705 ± 0.036	0.212 ± 0.027	17.6 ± 2.7	1.77 ± 0.17	0.0284 ± 1×10^{-4}	813 ± 105	1128 ± 288			$4.35 \pm 0.76 \times 10^{-4}$	$-5.00 \pm 2.36 \times 10^{-3}$	10 ± 2

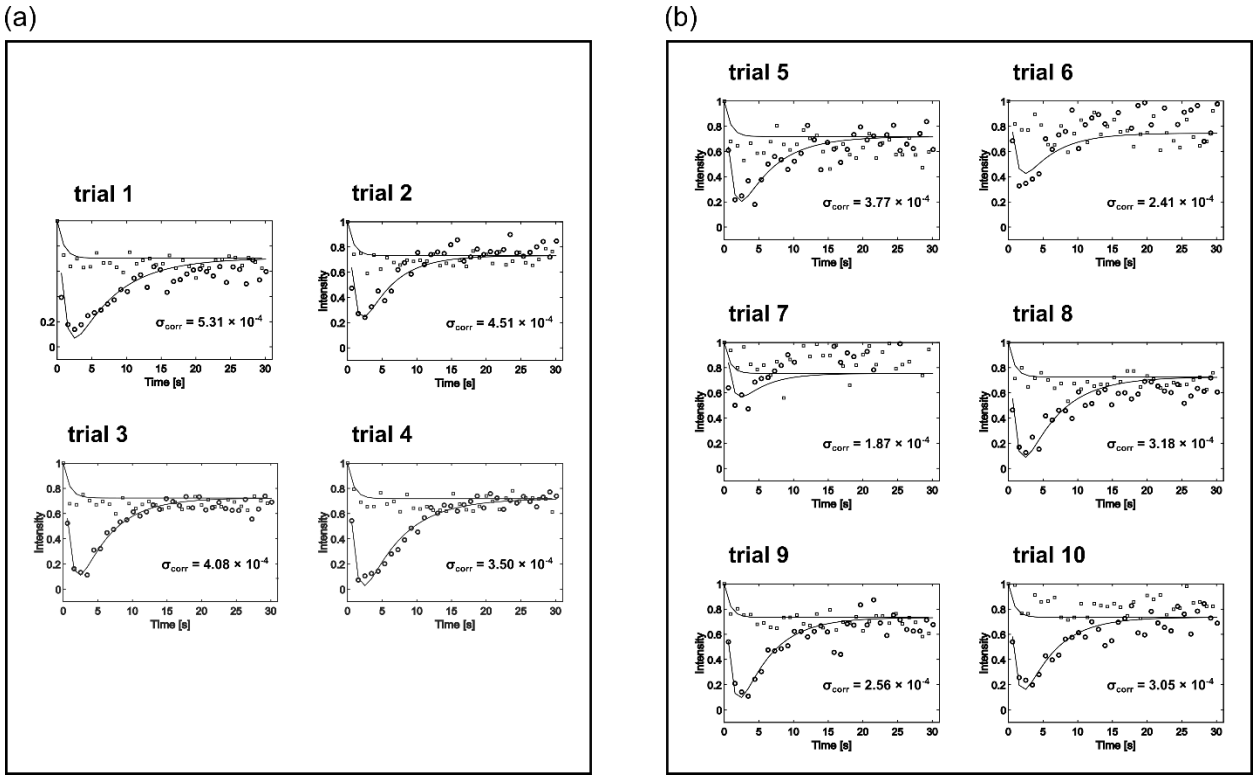

Figure A.8 NOE buildup curves of maximum ^{19}F signals for all the experimental trials shown in Table A.4. The maximum values from each scan are normalized with the maximum of the first non-hyperpolarized scan and shown as intensities. The apparent σ was fitted with the ε_{corr} characterized in real time with the dual-channel spectrometer for a preloaded sample of 60 mM TFBC in the (a) absence and (b) presence of 1.8 mM trypsin. Data points acquired after samples were mixed with hyperpolarized water and after the decay of hyperpolarization are shown as circles and squares, respectively.

A.3.3. Empirical Support for Simulation

The NOE buildup curves from selected experiments measured with the dual-channel spectrometer were displayed in Figure A.9 to demonstrate the change in NOE buildup upon when ε is near 1000. The maximum NOE buildup was at 0.2 for free TFBC and decreased to 0.4 in the presence of trypsin. The predicted result from the simulation was in alignment with this empirical observation.

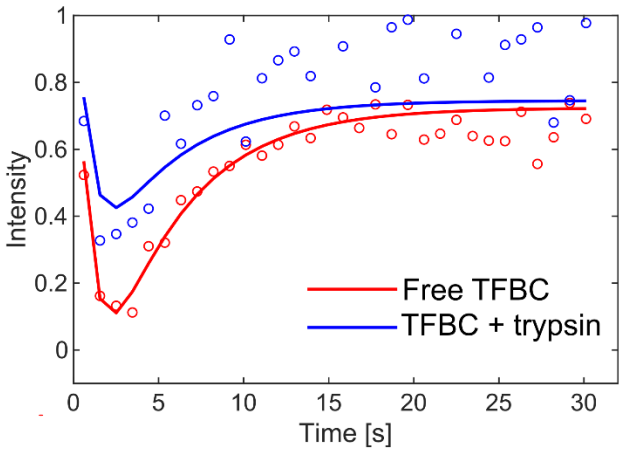

Figure A.9 Comparison of ^{19}F NOE buildup curves for a preloaded sample of 60 mM TFBC in the absence (red) and presence (blue) of 1.8 mM trypsin measured with the dual-channel spectrometer. Experimental trials with similar corrected ε of 1014 (red) and 1025 (blue) are compared. The comparison is drawn here to support predication made from the simulation on the effect of water signal enhancement.

A.4. References

(1) Dalvit, C.; Fogliatto, G.; Stewart, A.; Veronesi, M.; Stockman, B. WaterLOGSY as a Method for Primary NMR Screening: Practical Aspects and Range of Applicability. *J. Biomol. NMR* **2001**, *21* (4), 349–359.